CHALMERS

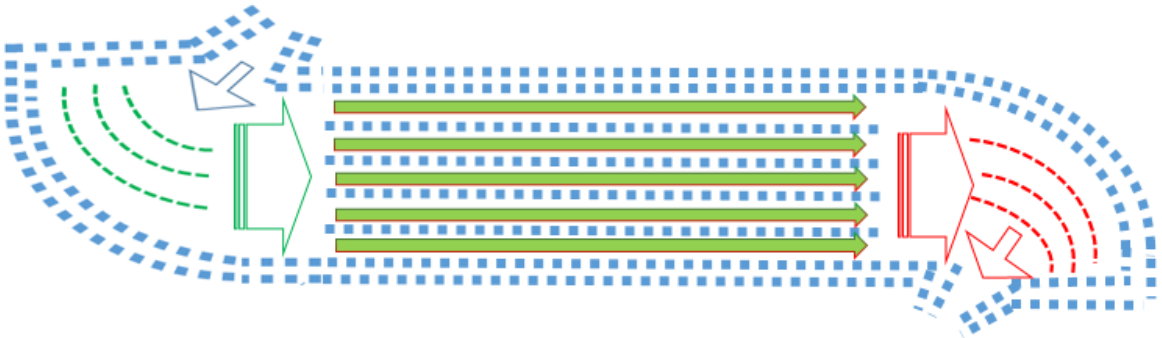

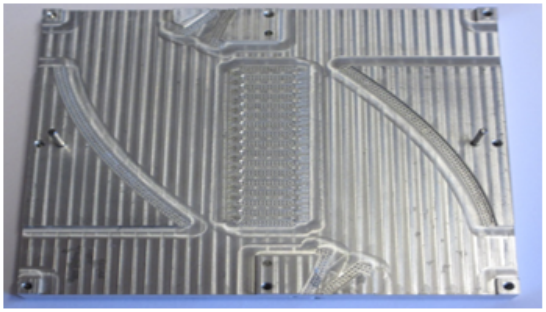

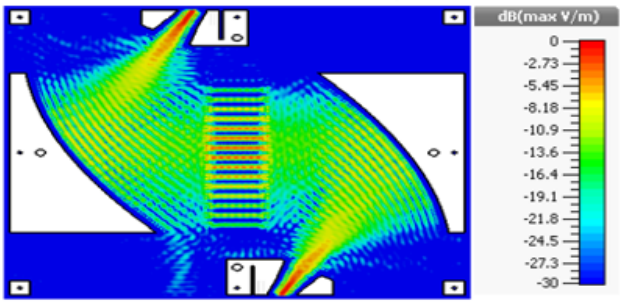

Millimeter-Wave Spatial Power Splitting and Combining for use in Gap-Waveguide-Integrated Grid Amplifiers and Antenna Arrays

Master's Thesis in Communication Engineering

Waqar Ali Shah

Department of Signals and Systems
Chalmers University of Technology
Gothenburg, Sweden, 2015.

Millimeter-Wave Spatial Power Splitting and Combining for use in Gap-Waveguide-Integrated Grid Amplifiers and Antenna Arrays

CHALMERS
UNIVERSITY OF TECHNOLOGY

MASTER's THESIS
as part of mandatory clauses in
fulfillment of Master's Degree from the
Chalmers University of Technology, Gothenburg, Sweden

by

Waqar Ali Shah
Antenna Systems Division,
Department of Signals and Systems

September, 2015

Millimeter-Wave Spatial Power Combining for use in Gap-Waveguide-Integrated Grid Amplifiers and Antenna Arrays / by
Waqar Ali Shah. - Gothenburg : Chalmers University of Technology, 2015.

This thesis is carried out under supervision of:
Dr. Marianna Ivashina, Associate Professor.
Dr. Rob Maaskant, Assistant Professor.
Dr. Ashraf Uz Zaman, Assistant Professor.

Examiner:
Dr. Per-Simon Kildal, Professor, Head of Division.

Keywords: Spatial power combiner / offset reflector / feed horn / gap waveguides / excitation coefficient / transition.
Subject headings: Spatial power combiner/ offset reflector / excitation coefficient / gap waveguides / transitions.

Technical Report No. EX063/2015:
Antenna Systems Division, Department of Signals & Systems
Chalmers University of Technology,
SE-41296, Gothenburg, Sweden.
Telephone: +46 31 772 1000

Cover design: Waqar Ali Shah
Press: Chalmers Reproservice, Göteborg

The work presented in this thesis has been performed at Antenna Group, Department of Signals & Systems, Chalmers University of Technology, SE-41296, Gothenburg, Sweden.

I dedicate my thesis work to my family.

Acknowledgements

First of all, I would like to thank Dr. Marianna Ivashina, Dr. Rob Maaskant and Dr. Ashraf Uz Zaman for giving me the chance to do a Master Thesis project with them. I am very grateful for their continuous guidance throughout my thesis. They are very open for discussion and support for new ideas. Their expert guidance in different fields helped me a lot to develop new skills.

I would like to thank Prof. Per-Simon Kildal for supporting and examining thesis work. Also, giving valuable suggestions during periodic presentation meetings.

I would like to say thanks to my fellow Master Thesis student, Alhassan Aljarosha for giving suggestions during my thesis work.

Waqar Ali Shah, Gothenburg, September 2015

Abstract

Conventional power splitters and combiners employing substrate-based transmission lines suffer from both conductor and dielectric losses, in particular at mm-wave frequencies. These losses increase when the number of channels increase, thereby reducing the efficiency even further. The primary aim the thesis work is to minimize these losses by spatially power combining (or splitting) the electromagnetic fields. This is will be done in a planar fashion and be packaged at the same time using gap-waveguide technology.

Spatial power combining techniques are also used in grid amplifiers. A gap-waveguide packaged and integrated grid amplifier is therefore an interesting application to consider. Indeed, conventional grid amplifiers typically employ different feed networks including both dielectric lenses and polarizers, which are bulky and lossy and suffer from DC biasing problems. To overcome these problems, we propose to split and combine the power through a reflector-wall-based back-to-back gap waveguide structure.

First, an offset reflector wall has been designed and simulated in receive mode in which the reflector aperture is illuminated with a single large port and fields are analyzed at the focal point. The horn feed is designed on the basis of an encircled power analysis in the focal plane. The reflector wall is then illuminated by the designed feed and the resultant planar fields from this reflector are fed back into a second feed making up the back-to-back structure. The fields emanating from the offset reflector wall are equal in phase but tapered in magnitude. In order to more gradually taper the field leading to a more uniform amplitude distribution a slightly larger offset reflector wall has been designed. The planar waterfronts of the fields of the reflector couple into an array of waveguides using customized ridge gap-waveguide transitions. A fork shaped transition has been designed so that the edges of the walls of the waveguides do not appear abruptly in front of the planar fields. This ensures that the planar field divides and propagates into the waveguides with minimal reflection.

This work is important because it represents a low-loss power splitting and combining solution of mm-wave systems with S_{11} less than -10 dB that covers the frequency range from 74 GHz to 110 GHz. It also forms the basis for a mm-wave grid amplifier in gap waveguide technology.

Contents

1 Introduction **1**

1.1 Background and Motivation 1

1.2 Gap Waveguide Technology Concept 4

1.3 Brief Overview of the Thesis 6

2 Offset Reflector Wall Design and Receive Mode Analysis **9**

2.1 Introduction 9

2.2 Design and Simulation Results 10

2.3 Conclusion 12

3 Investigation of Optimal Amplitude Excitations for Waveguides-A Receive Mode Field Analysis **15**

3.1 Theory and Simulation results 15

3.2 Conclusion 19

4 Groove to Ridge Gap Waveguide Back-to-Back Power Combiner and Divider **21**

4.1 Design and Simulation of a Feed Horn 21

4.2 Design of Transition between Aperture of Offset Reflector Wall and Array of Waveguides 23

4.3 Simulation of Back-to-Back structure consisting of Waveguides and Transitions 27

4.4 Conclusion 30

5 Re-Design for Prototyping, Manufacturing, and Test Results 33

5.1 The Prototype Design 33

5.2 Manufacturing and Test Results 35

5.3 Conclusion 37

6 Conclusions and Recommendations 39

6.1 Conclusions 39

6.2 Recommendations 40

Appendix 41

A 41

Bibliography 43

Chapter 1

Introduction

In this chapter, drawbacks related to the use of conventional power combining and splitting techniques in grid amplifiers are discussed. The motivation for the use of the both spatial power combining and the gap waveguide technology is described. Finally, a brief summary of the thesis is provided.

1.1 Background and Motivation

The term "spatial power combining" is a method in which fields are combined in free space. A similar term "quasi-optical power combining" has also been used but it is more based on lens and mirror elements that are incorporated inside spatial combiners [1], [2]. The spatial power combiner is used for coupling the fields into a grid of amplifiers in which multiple numbers of solid-state Monolithic Microwave Integrated Circuit (MMIC) amplifiers are stacked together in the form of an array to increase the overall amplifier power-handling capability. Previously, many spatial power and optical power combining techniques have been presented which were based on conventional corporate feeding networks, dielectric lenses and bulky horn antennas [3]. These devices had issues like low radiation efficiency and power losses [4], diffraction losses in the lenses and the required compensation for phase imbalance at the last stage combiner [5]. At millimeter-wave frequencies the operating band is relativity narrower because of higher ohmic losses at these frequencies [6].

Previously in [7], 36 Watts (W) continuous wave output power has been achieved by combining 272 MMICs at 61 GHz. The concept employ a sectoral horn feed and focusing lens with an array of 17 linear dipole elements. An X band, 120 W amplifier at 8 GHz which was comprised of a rectangular waveguide feeding structure and 24 MMICs amplifiers [8]. Another 25 W (50 W) amplifier at 34 GHz was demonstrated which consisted of a pyramidal horn feed and a 45 (98) double sided active patch antenna array [9]. A lens focusing using horn feed power combiner/splitter was designed at 37 GHz to achieve 5 W at the output [10]. Current research is being carried out to achieve a saturated output power of 600 W in C band by 16 GaAs Field-Effect Transistors (FETs) and by using an array of tapered patch antennas, as a results of which this system is very narrow band, (i.e.) 6 GHz [11]. The packaging and thermal issues are still a major issue as well as the biasing and cooling of the amplifiers [12].

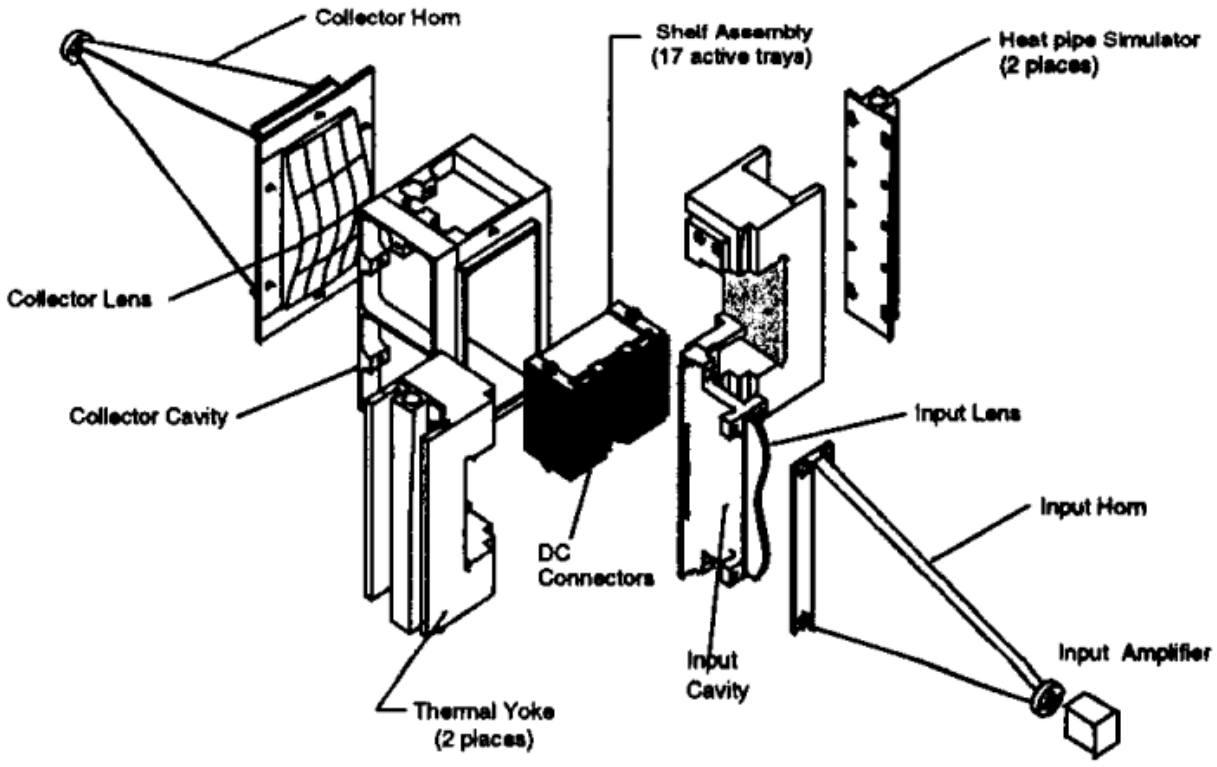

Figure 1.1: A 36 W, V-band, solid-state source [7].

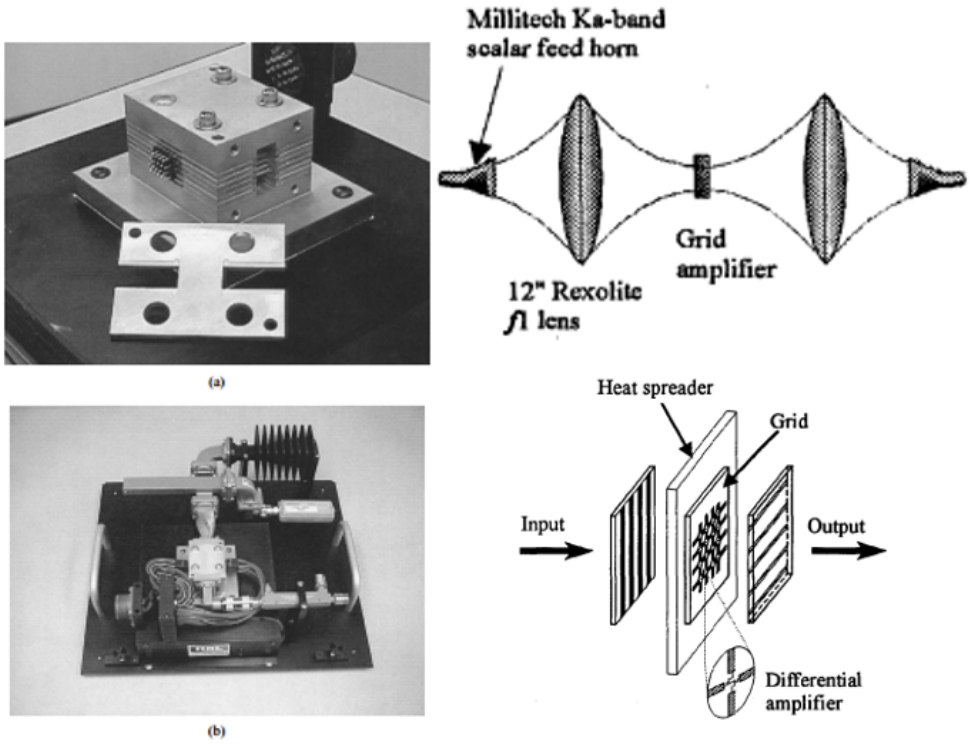

Figure 1.2: A 120-W X-band spatially combined solid-state amplifier (Left) [8] and a 5-watt, 37-GHz monolithic grid amplifier (Right) [10].

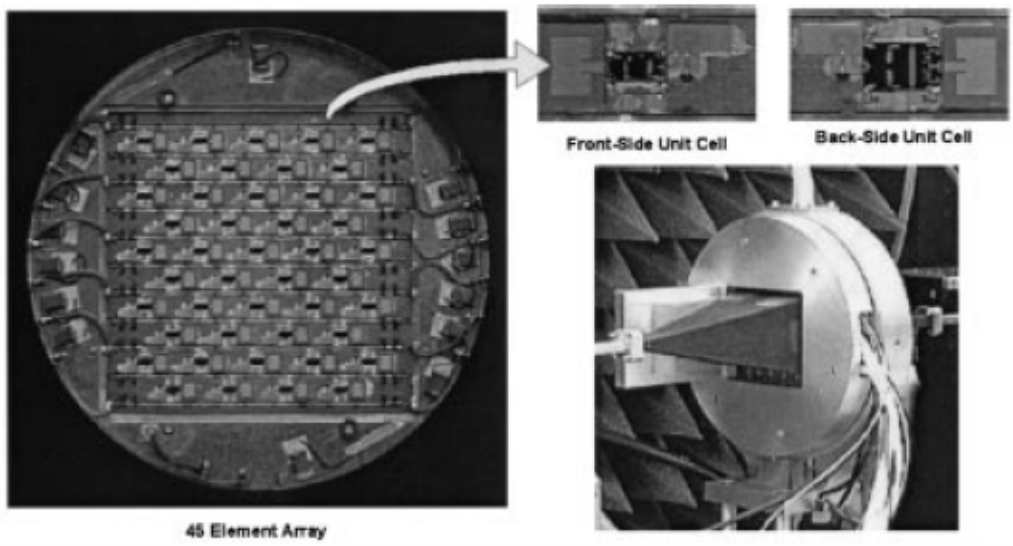

Figure 1.3: A 25 watt and a 50 watt Ka-band quasi-optical amplifier [9].

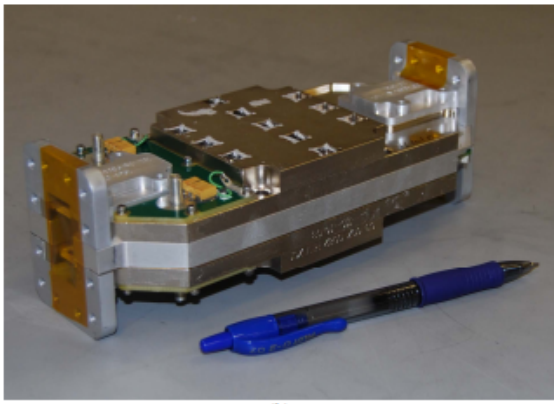

Figure 1.4: A 600-W C-band amplifier using spatially combined GaAs FETs [11].

To overcome the above-mentioned problems, it is proposed to use an offset reflector-wall-based spatial power combining technique as shown in Fig. 1.5. The concept is based on having a reflector wall which is illuminated by an offset feed in combination with an array of waveguides at the large aperture of the reflector [13], [14]. Power is divided or combined at the first stage over the air with minimal losses. This method is wide band. The complete structure is based on gap waveguide technology to suppress cavity resonances at high frequencies [15]. With this method of power combining, the output power will be less affected in case of few malfunctioning components [16]. Due to these advantages, a reflector-wall-based spatial power combiner can easily be used for a grid of amplifiers. The long term vision is that slot antenna arrays or grid amplifiers based on gap waveguide technology can be designed based on the spatial power combiner mentioned in this thesis (see e.g. [17]).

1.2 Gap Waveguide Technology Concept

With the passage of time, radio frequency allocation is shifting towards W band for high speed communication [18]. This reduces the size of microwave components at higher frequencies challenging the designers and manufacturers to work with higher precision. Assembling of the components is also challenging as minor misalignments and poor electric contact between the metal blocks cause huge degradation in performance as the wavelengths at the millimeter-wave frequencies.

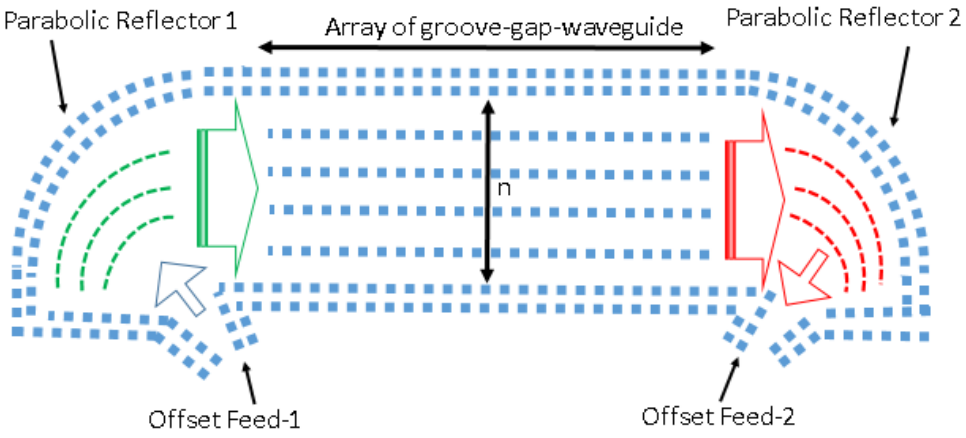

Figure 1.5: Illustration of offset reflector wall based spatial power divider and combiner.

To cater the issues related to field leakages between metal contact surfaces at millimeter frequencies, gap waveguide technology has been introduced [15], [19]-[20]. The concept of gap waveguide technology comes from the idea of soft and hard surfaces which has led to corrugated surfaces used in antennas [18], [21]. This new technology consists of two parallel Perfect Electric Conductor (PEC) planes while a ridge or groove is made within the bed of pins on one of the plates as shown in Fig. 1.6. This bed of periodic pins acts as Perfect Magnetic Conductor (PMC) surface [19], [22]. The gap between the PMC and PEC surfaces establishes a cut-off frequency region for propagating EM fields [23]. In these structures, fields propagate along the groove or ridge without leaking in other directions. There is no contact between top and bottom metal plates which makes it suitable to manufacture at mm-Wave frequency range and above. Three different types of gap waveguide technologies include the groove, ridge, and microstrip gap waveguide [24]. In the current work, the ridge gap waveguide has been implemented for reasons as discussed in Chapter 4.

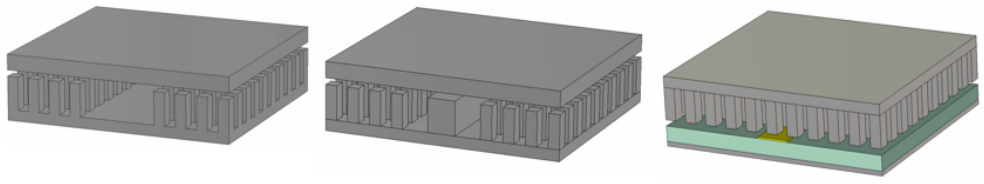

Figure 1.6: Groove (Left), Ridge (Middle) and microstrip (Right) gap waveguide technology.

To design a gap waveguide structure, we first examine the dispersion diagram of single unit cell containing the pin. In Fig. 1.7 it is shown that there are no modes present from

70 GHz to 140 GHz ($L = W = 0.3$mm, $H = 0.81$mm and $S = 0.19$mm). These pins are periodically placed at equidistant positions and can be used to replace traditional metal walls in waveguides. The pins are designed based on the study presented in [23], [25]-[28].

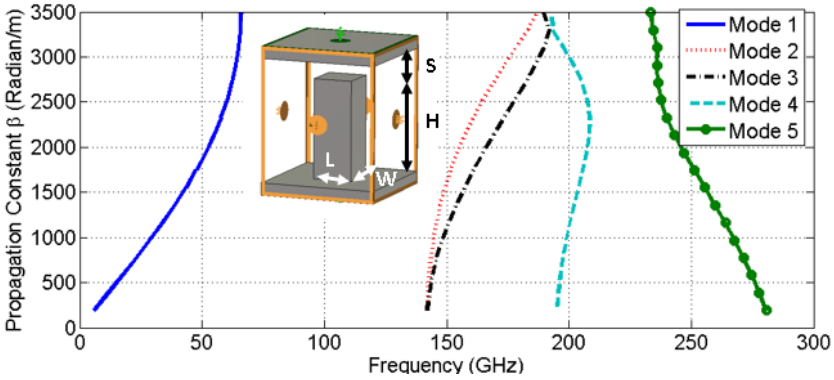

Figure 1.7: Dispersion diagram for a unit cell containing a pin.

As mentioned before, the problems of good electrical contact and alignment between the waveguide blocks are solved by means of gap waveguide technique. Several passive millimeter wave components such as filters and antennas have been recently designed based on the gap waveguide technology to demonstrate the above mentioned mechanical flexibility [17], [29]-[32]. Also the gap waveguide technology is very suitable for RF packaging [33]-[35], which plays an important role in integrating RF electronics with the antennas or waveguide modules. The gap waveguide technology is also very suitable for micro-machining which a way of manufacturing waveguide components above 100 GHz which plays an important role in integrating RF electronics with the antennas or waveguide modules [36].

1.3 Brief Overview of the Thesis

A brief overview of the thesis is provided below:

- Chapter 2 discusses the design of the offset reflector wall. The reflector wall is simulated in receive mode in which planar EM fields that are well-matched are radiated by the array of waveguides and are incident to the aperture of the reflector. Then, these fields converge to the focal point of the offset reflector wall. Power received at the focal plane is analyzed by exciting the waveguides with equal amplitudes.

- Chapter 3 discusses the effects of assuming optimal amplitude weights during receive mode analysis. To this end, we excite the waveguides one by one with unit amplitude, the field is measured at the feed and then the optimal amplitude coefficients are determined for the waveguide ports based on these fields. The power received at the focal plane is analyzed by assuming optimum amplitude excitations at the waveguide ports.

- Chapter 4 describes the results for the transmit mode the results of which are used to design an offset feed that realizes well matched EM fields from the reflector planar fields to the array of waveguides. Subsequently, a back-to-back structure is designed based on this transition. The optimization of the transition between the reflector and the waveguides is also presented, which was needed due to the otherwise high reflections from the waveguides.

- Chapter 5 discusses measurement results of the back-to-back structure with a parabolic reflector wall. Effects of spacing between the waveguide walls in the prototype gap waveguide and the conventional metallic structure is also compared. The measurement results of a back-to-back structure have also been discussed.

- Chapter 6 concludes the present work and recommends the direction for future work.

Chapter 2

Offset Reflector Wall Design and Receive Mode Analysis

In this chapter, an offset cylindrical reflector wall has been designed using PECs. In receive mode, the planar EM fields that are radiated by the array of waveguides and are incident to the aperture of the reflector. Then these fields converge to the focal point of the offset reflector wall. A numerical analysis has carried out at the focal plane by exciting the waveguides with equal amplitudes.

2.1 Introduction

There are different types of reflectors, for example: prime focus, offset feed, Cassegrain and Gregorian. Among them, the offset feed reflector is more suitable to match fields originating from waveguides placed at the aperture of the reflector. because there is no disturbance to the EM fields in front of the aperture of the reflector due to feed blockage and struts. The offset reflector wall has been designed using parabola (2.1) [37]. The corresponding general geometry is shown in Fig. 2.1.

$$z = \frac{y^2}{4F} - F \tag{2.1}$$

In Fig. 2.1, F is the focal length along z-axis, h is the height of the center of the reflector along the y-axis. Total height of offset reflector wall is $D/2$ where D is diameter of parent

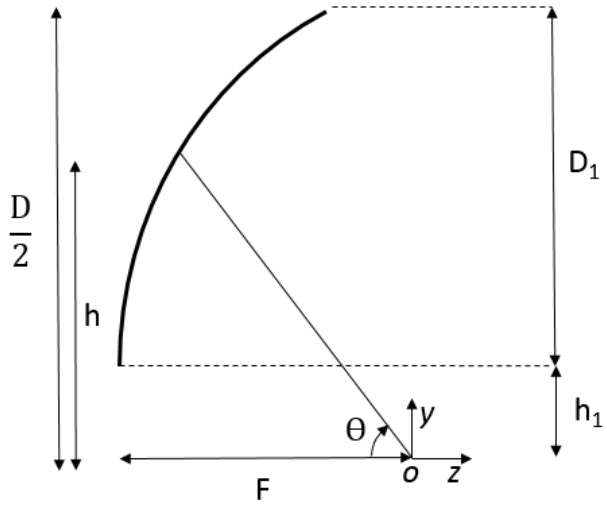

Figure 2.1: General diagram of offset reflector antenna design [37].

paraboloid. Half of the diameter $D/2 = D_1 + h_1$ is the total height of the reflector from the focal axis. Where D_1 is diameter of the cylinder, h_1 is offset height and angle Θ is the angle from the focal axis to the center of the offset reflector.

2.2 Design and Simulation Results

We first perform a receive mode analysis. The diameter of the reflector wall is kept equal to 9 waveguides because it makes the dimensions near to 10λ in-order to receive and transmit planar waves from the aperture. The walls of the waveguides and reflector have been designed with PEC surfaces. Each waveguide width is kept 2.54 mm according to the standard W-band waveguide width and 0.22 mm wall thickness between waveguides makes 25.06 mm total dimension for aperture of the reflector D_1. The focal length F is 13.08 mm and the offset height h_1 is 3 mm below the last waveguide. Using these parameters, the offset reflector wall with $0.46\frac{F}{D}$ ratio and Θ is 60 degrees towards the center of reflector from focal point has been designed in MALTAB and imported into CST. In CST, the reflector has been thickened with PEC walls and placed in front of the waveguides as shown in Fig. 2.2. The structure is not closed with PEC materials at the top and bottom planes because the electric boundary condition is assigned in CST MW-Studio.

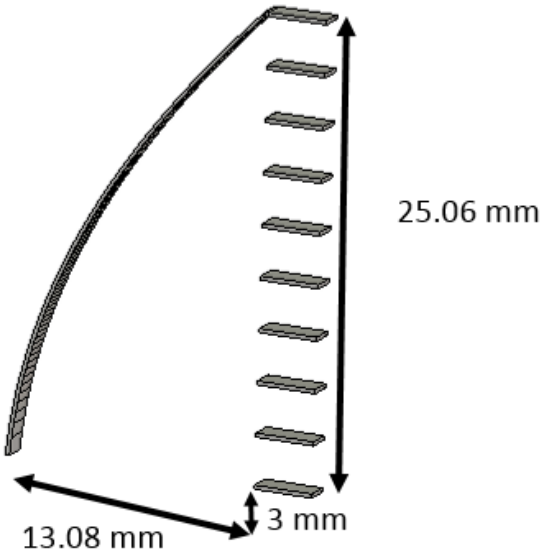

Figure 2.2: Designed offset reflector wall and waveguides in CST-MW Studio for receive mode analysis.

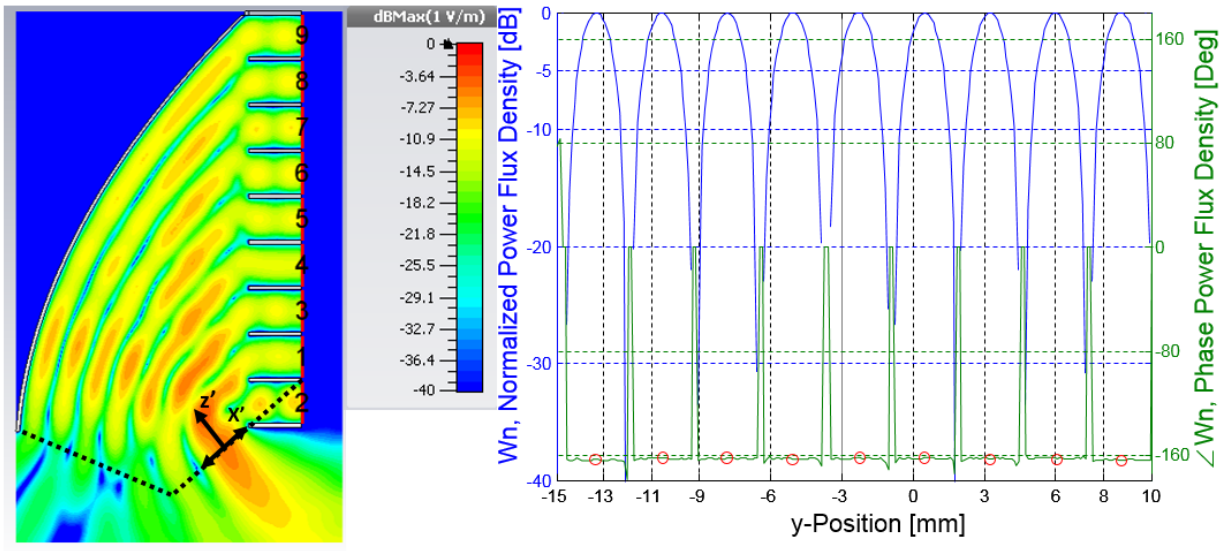

Figure 2.3: Magnitude plot (Left) in CST-MWS in receiving mode using equal excitation coefficients and phases at the waveport (Right).

Each of the waveguides has been excited by their waveports at the same time. The EM field generated from the waveguides when excited by equal amplitudes and phases are shown in Fig. 2.3. These waves are reflected back from the reflector wall and converge at focal

point. The power density vector $\underline{S}$ at each point of focal plane *x'-y'* and normal $\underline{\hat{z}}$' vector is directed towards the center of the reflector wall from the focal point. The time-averaged power density vector has been calculated from the cross product of the $\underline{E}$ and $\underline{H}$ vector components in the focal plane:

$$\underline{S} = \frac{1}{2}\mathrm{Re}\{\underline{E} \times \underline{H}^*\} \tag{2.2}$$

Integral of the time-averaged power density along the normal to the focal plane over a truncated aperture gives the received power:

$$P_{\mathrm{rec}} = \iint_A \underline{S} \bullet \underline{n}\, ds = \frac{1}{2}\mathrm{Re}\{ \iint_A \underline{E} \times \underline{H}^* \bullet \underline{n}\, ds\} \tag{2.3}$$

Where 'A' is the aperture of the focal plane whose truncated size depends on the frequency. A is determined for the lowest frequency.

The received power P_{rec} gives an estimation of the power captured at the focal plane with ascending position as shown in Fig. 2.4 [38]-[39]. This graph also shows the percentage of power captured with ascending electrical distance from the center point on the focal plane. It shows that 83.85% of power has been received at 1λ radial distance as compared to optimally (Chapter 3) excited waveguides. The rest of the power is lost in spillover. On the basis of this result, the opening of waveguide horn antenna was kept 1.6λ at the lowest frequency in the beginning but later on, results are more improved with 2λ opening. The feed has been designed using a transmit mode simulation as explained in Chapter 4.

2.3 Conclusion

This chapter describes the EM waves that have been simulated and analyzed in the receiving mode. After the reflection from the reflector wall, the EM fields converge at the focal point. The analysis has been done at the focal plane which is important for the feed design. Graphs show the maximum captured power with in a certain radial distance from the focal point which is within almost 1λ, 83.85% of power has been received.

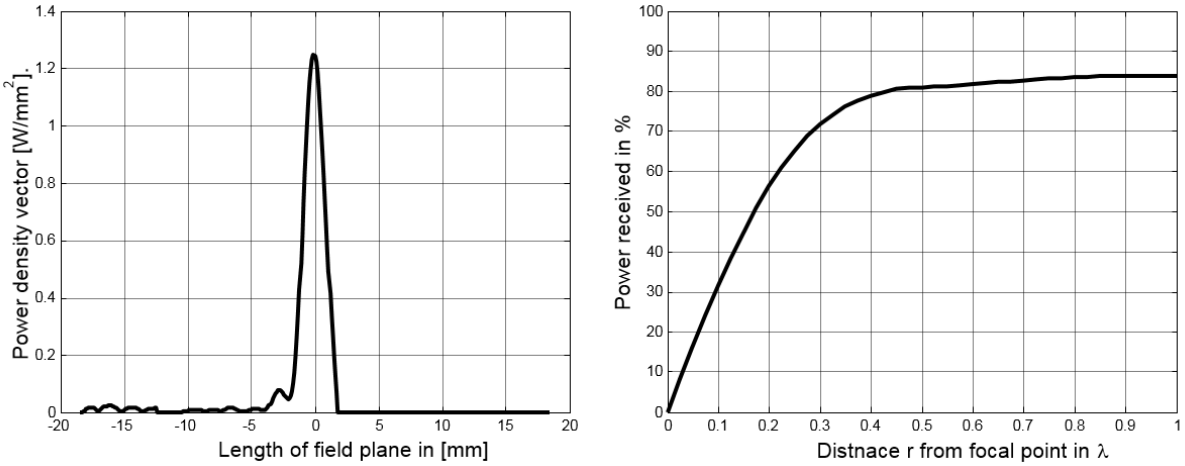

Figure 2.4: Power density vector [W/mm^2] plot in the focal plane (Left) and Percentage of power versus the required aperture radius in the focal plane (Right).

Chapter 3

Investigation of Optimal Amplitude Excitations for Waveguides-A Receive Mode Field Analysis

In this chapter, the optimal amplitude excitations for the waveguides has been derived during the receive mode analysis and been used for the optimal feed design. To this end, the presented array of waveguides has been excited one-by-one with unit amplitude and excitation coefficients have been found theoretically for the waveguides by measuring the fields at the feed [41]-[42]. Afterwards, the waveguide ports are excited by the resultant optimum amplitude excitations and an analysis has performed at the focal plane to measure the amount of power captured with ascending radial position from the focal point.

3.1 Theory and Simulation results

The integral in (3.1) of the power density normal to the focal plane over a truncated aperture gives the total power captured. In order to determine individual excitation coefficients W_n for n = 1, ..., 9, each of the waveguides in Fig. 3.1 is excited one by one. E- and H-fields have measured at the aperture located at the superposition of the individual fields $\underline{E}^n$, $\underline{H}^n$, i.e.,

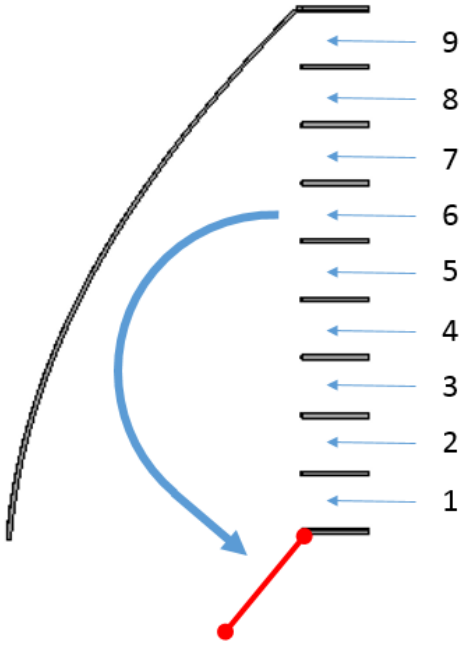

Figure 3.1: One-by-one waveport excitation in receiving mode to measure the E and H fields.

$$\underline{E} = \sum_{n=1}^{9} W_n \underline{E}^n, \;\; \underline{H} = \sum_{m=1}^{9} W_m \underline{H}^m \text{ Where } m, n = 1 \ldots 9, . \tag{3.1}$$

Using (2.2), the received power becomes:

$$P_{\text{rec}} = \frac{1}{2}\text{Re}\Big\{ \iint_A \Big[\sum_{n=1}^{9} W_n \underline{E}^n \times \sum_{m=1}^{9} W_m^* (\underline{H}^m)^* \Big] \bullet \underline{\hat{n}}\, ds \Big\} \tag{3.2}$$

Where 'A' is aperture taken to be 0.8λ in size (determined for the lowest frequency). Rearranging yields.

$$P_{\text{rec}} = \frac{1}{2}\text{Re} \sum_{n=1}^{9} \sum_{m=1}^{9} W_n \iint_A \underline{E}^n \times (\underline{H}^m)^* \bullet \underline{n}\, ds \; W_m{}^* = \frac{1}{2}\text{Re}\big\{ \underline{W}^T \; P \; \underline{W}^* \big\} \tag{3.3}$$

$$\text{Where } P_{nm} = \iint_A \underline{E}^n \times (\underline{H}^m)^* \bullet \underline{\hat{n}}\, ds$$

Where we note that (cf. Appendix-A)

$$P_{\text{rec}} = \frac{1}{2} \; \underline{W}^T \; \text{Re}\big\{P\big\} \; \underline{W}^* = \frac{1}{2} \; \underline{W}^H \text{Re}\big\{P\big\}^T \; \underline{W} \tag{3.4}$$

When waveguides are excited in the same parallel plate waveguides that are used in Chapter 2, the total input power P_{in} becomes (for well-matched waveguides without mutual coupling) at the input of waveguides and power received P_{rec} at the focal plane.

$$P_{\text{in}} = \sum_{k=1}^{9} |W_k|^2 = |W_1|^2 \ + \ldots + \ |W_9|^2 \ = \underline{W}^H \underline{W} = [W_1 \ldots W_9] \begin{pmatrix} W_1 \\ \vdots \\ W_n \end{pmatrix}. \tag{3.5}$$

In order to find the optimal excitation coefficients $\underline{W_{\text{opt}}}$, we first define the cost function $\frac{P_{\text{rec}}}{P_{\text{in}}}$ that needs to be maximized with respect to $\underline{W}$:

$$\frac{P_{\text{rec}}}{P_{\text{in}}} = \frac{\frac{1}{2}\underline{W}^H \ A \ \underline{W}}{\underline{W}^H \underline{W}} \tag{3.6}$$

where A is replaced by $\text{Re}\{P\}^T$. Accordingly,

$$\max_{\underline{W}} \left(\frac{P_{\text{rec}}}{P_{\text{in}}} \right) => \partial_{\underline{W}^H} \left(\frac{\underline{W}^H \ A \ \underline{W}}{\underline{W}^H \underline{W}} \right) = 0 \tag{3.7}$$

Which can be written as

$$\frac{\underline{W}^H (\underline{W} A \underline{W}) - (\underline{W}^H A \underline{W}) \underline{W}}{(\underline{W}^H \underline{W})^2} = 0 \tag{3.8a}$$

$$\underline{W}^H (\underline{W} A \underline{W}) - (\underline{W}^H A \underline{W}) \ \underline{W} = 0 \tag{3.8b}$$

$$(\underline{W}^H A \underline{W}) \underline{W} = (\underline{W}^H \underline{W}) A \ \underline{W} \tag{3.8c}$$

Yielding

$$\left(\frac{\underline{W}^H A \underline{W}}{\underline{W}^H \underline{W}} \right) \underline{W} = A \underline{W} \tag{3.9}$$

This is recognized to be same as

$$\left(\frac{P_{\text{rec}}}{P_{\text{in}}} \right) \underline{W} = A \underline{W} \tag{3.10}$$

which is equal to the Eigen value problem of the form $A\underline{x} = \lambda \underline{x}$, i.e.,

$$A \underline{W} = \left(\frac{P_{\text{rec}}}{P_{\text{in}}} \right) \underline{W} \tag{3.11}$$

Maximizing $\frac{P_{\text{rec}}}{P_{\text{in}}}$ is equivalent to Eigen vector corresponding to the largest Eigenvalue of the matrix 'A'. The optimal waveguide excitation coefficient vector $\underline{W_{\text{opt}}}$ is the principle Eigen vector of A, which has been plotted in Fig. 3.2. The determined $\underline{W_{\text{opt}}}$ is used to excite the waveports and the has been simulated and shown in Fig. 3.3 in receiving mode. Similarly to Section 2.2, the power density and the percentage of power received has been calculated and been plotted at the focal plane in Fig. 3.4 where more than 90% of the power has been received within 1λ radial position from the focal point.

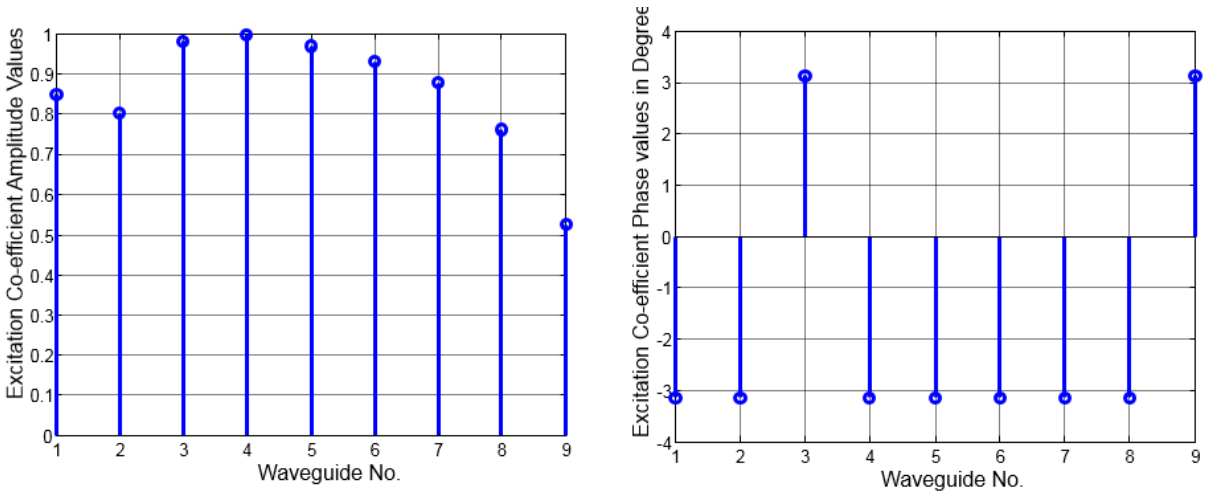

Figure 3.2: Optimal excitation coefficients for the waveguides (Left) and corresponding phases (Right).

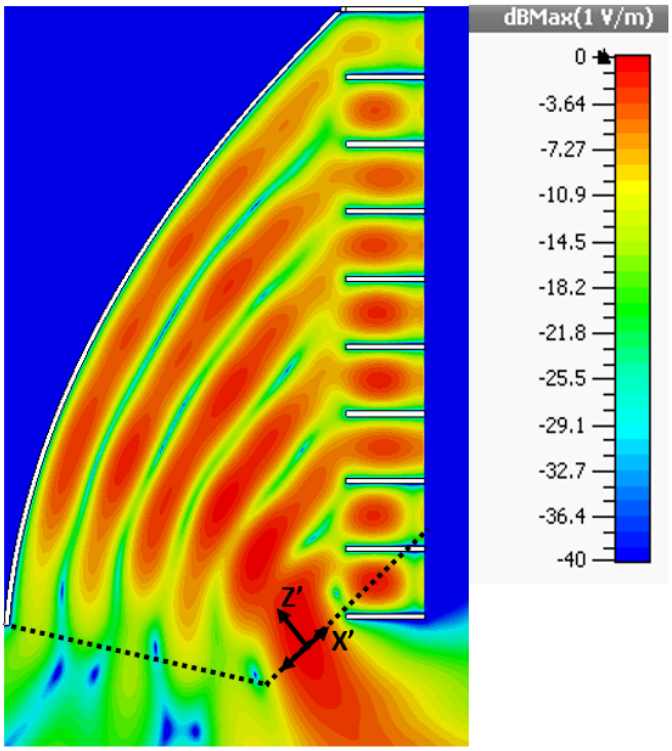

Figure 3.3: Designed reflector wall and waveguide in CST-MW Studio software for receiving mode analysis with optimal excitation co-efficients.

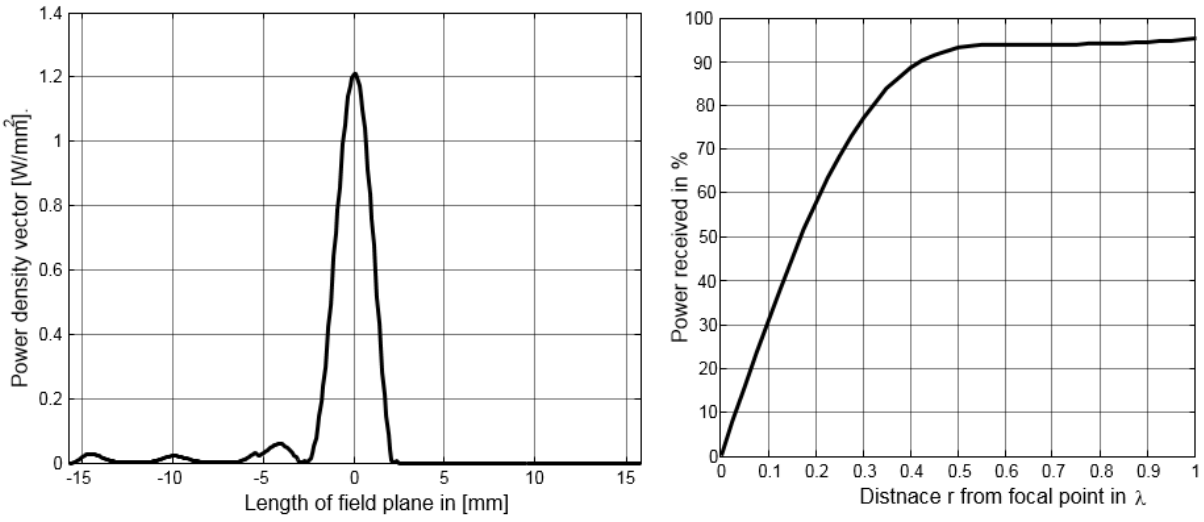

Figure 3.4: Power density vector [W/mm^2] plot in the focal plane (Left) and percentage of power versus the required aperture radius in the focal plane (Right).

3.2 Conclusion

The optimal excitation coefficients have been determined for the waveguides operating in the receive mode excitation. The captured power at the focal point is more than the result when exciting the waveguides with equal magnitudes and phases. In conclusion, newly found excitation coefficients avoid the use of equal excitation at the waveguides ports to give more power received at the focal point.

Chapter 4

Groove to Ridge Gap Waveguide Back-to-Back Power Combiner and Divider

A transmit mode analysis on the EM fields is performed in this chapter. The feed horn is designed for an offset reflector wall on the basis of the receive mode analysis (Chapter 2). Furthermore, the transmit mode fields have been coupled from the aperture of the offset reflector wall to the receiving waveguides via well-matched transitions using ridge gap waveguide technology. Finally, a back-to-back structure has been simulated.

4.1 Design and Simulation of a Feed Horn

The receive mode analysis in Chapter 2 has helped us in providing initial dimensions of the feed horn for the transmission of EM fields as shown in Fig. 4.1. The feed horn opening is kept 2λ for which more than 90% of power has been captured. The offset parabolic reflecting wall is designed in gap waveguide technology with parameters: Diameter of offset reflector = 55 mm; s/2 = 36.3 degrees; Offset height = 10 mm, and; Focal length = 32.5 mm. Hence, F/D = 0.59. Initially, a long PEC waveguide bend was designed and placed in-between the horn and the port. This made structure unnecessarily large. Then the bend was reduced and converted into the pin structure in accordance with the gap

waveguide technology. Still, more optimization and adjustments of the pins were needed at the a starting point of the horn because it was the most sensitive part of the horn. Ultimately, the bend was adjusted by moving the pins to reduce any further leakage and reflections. For the transmit mode simulation, the feed horn is excited at its waveport

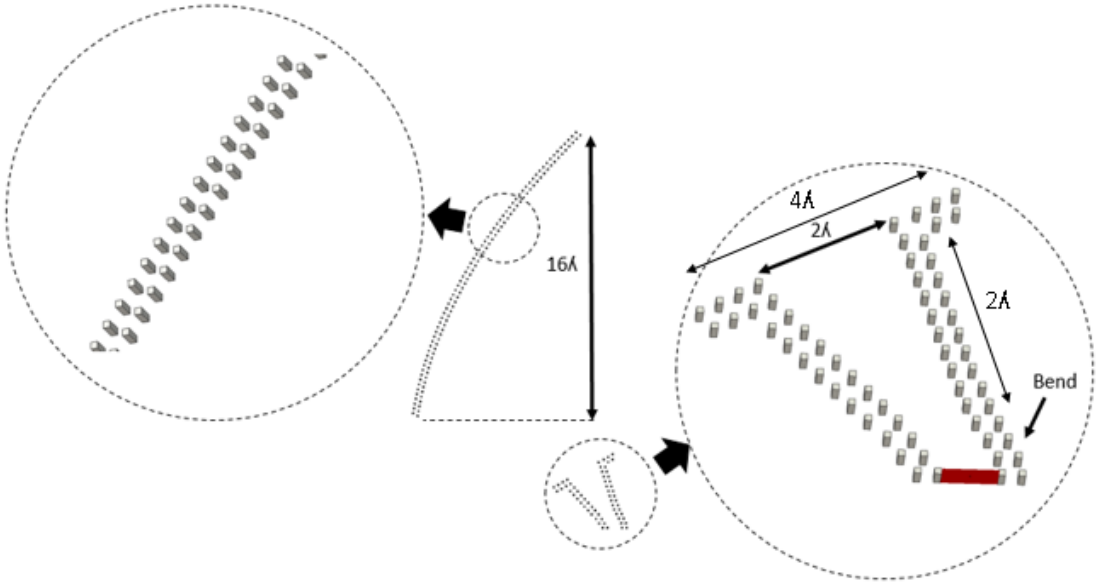

Figure 4.1: Designed feed and offset reflector wall in gap waveguide technology.

(Fig. 4.1). The fields are reflected by the reflector wall to transform into planar waves as shown in Fig. 4.2. The fields are seen to perfectly reflect from the reflector wall and are transmitted towards the far-field region. The spillover at the edges are at the level of -30 decibels. In Fig. 4.3 we can see the S_{11} plot at the waveport which shows that the reflection coefficient is low in the whole 75-110 GHz frequency range.

In order to examine the insertion loss along with the reflection coefficient, another offset reflector wall and its feed have been placed symmetrically in a back-to-back structure as shown in Fig. 4.4. The EM fields which emanate from the aperture of the left offset reflector wall reflects back from the right-side reflector wall and converges towards the focal point of the 2^{nd} reflector wall. The amplitude and phase fields plots can been in Fig. 4.5. It shows that the fields are propagating with the same phase and tapered amplitude pattern smoothly. Similarly, the S_{11} and S_{21} can be seen in Fig. 4.6, where the S_{21} is degraded only in the 70-78 GHz frequency range but it covers rest of the W-band.

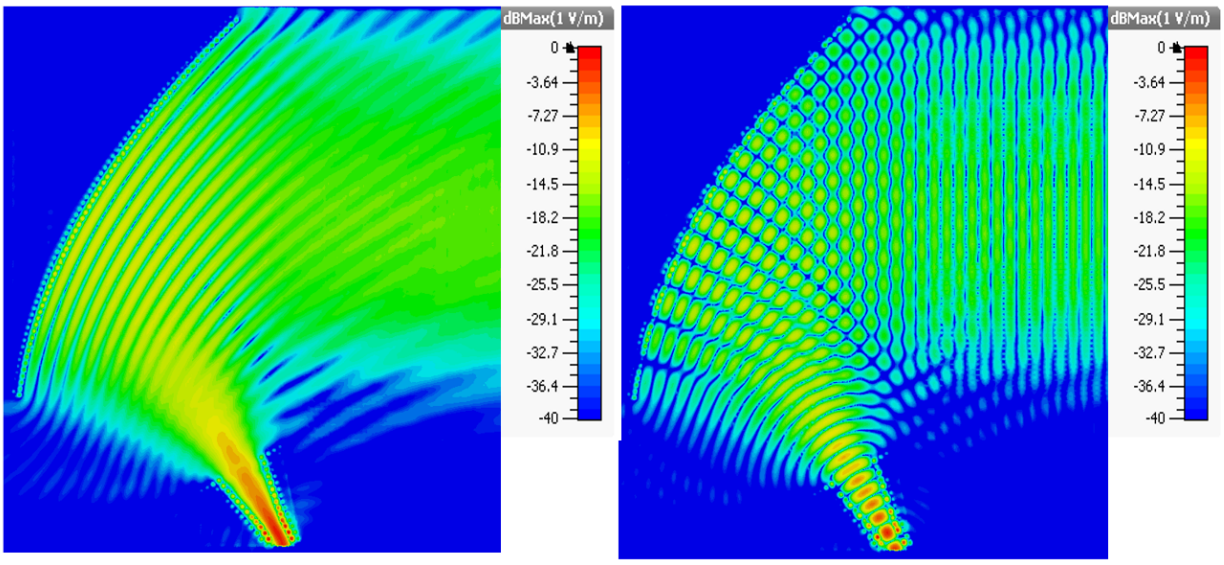

Figure 4.2: Simulation of offset reflector: Absolute magnitude plot (Left) and absolute phase plot (Right) of E-Field component.

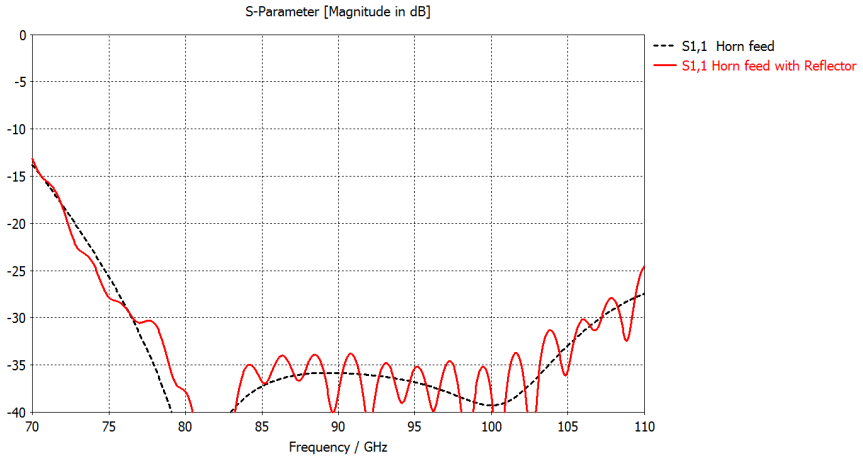

Figure 4.3: S-parameter plot for feed horn and with offset reflector wall antenna.

4.2 Design of Transition between Aperture of Offset Reflector Wall and Array of Waveguides

In Sec. 4.1 the reflectors and feeds have been designed in a back-to-back configuration and fields have received in receiving horn antenna without using any waveguides in the middle open space. In order to capture the plane waves emerging from the aperture of

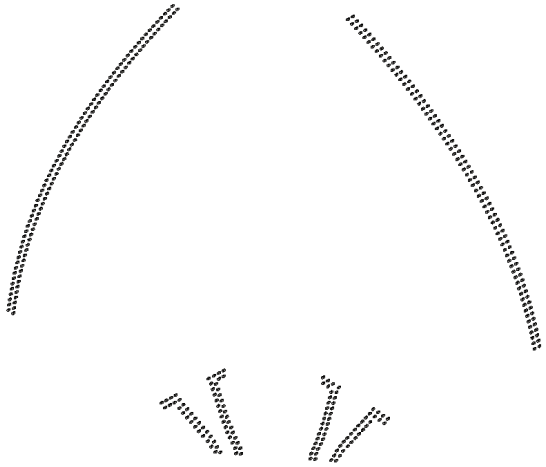

Figure 4.4: Designed feed and offset reflector wall in gap waveguide technology in a back-to-back configuration.

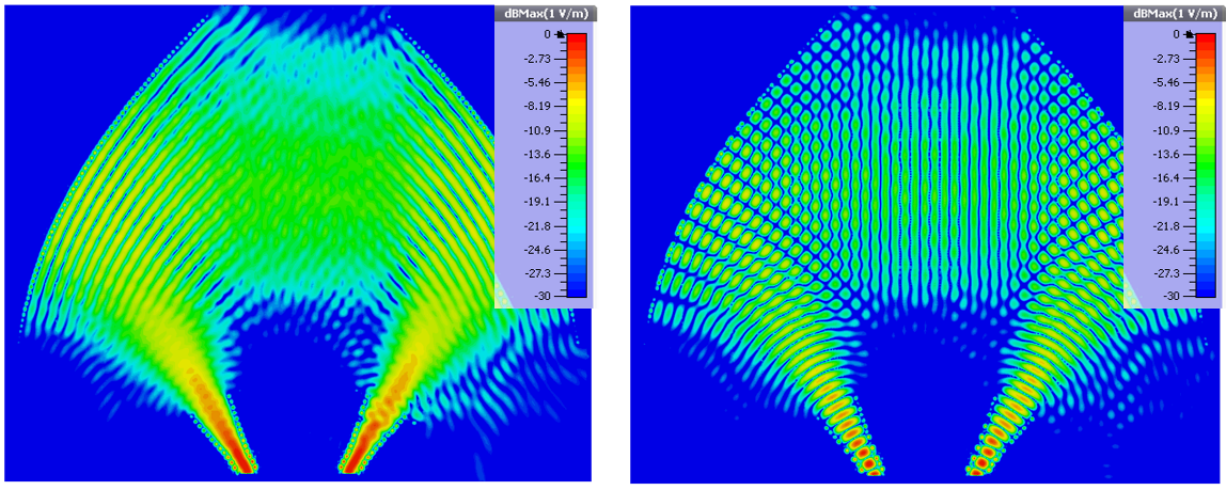

Figure 4.5: Simulation of an offset reflector wall in a back-to-back configuration: Absolute average magnitude plot (Left) and absolute phase plot (Right) of E-field component.

the offset reflector wall in the front of waveguides, an equivalent size of waveport has been placed in the front of the waveguides for the independent optimization simulations. The EM waves originating from a large waveport was required to couple to the waveguides as shown in Fig. 4.7. One method was by to use a ridge and the second was to use groove gap waveguide technology. None of them worked very well, i.e., tapering of the wall heights, gradual separation of ridges from the waveport to the waveguides and increasing width of ridges etc. High reflections remained from the walls of the waveguides as can be seen in

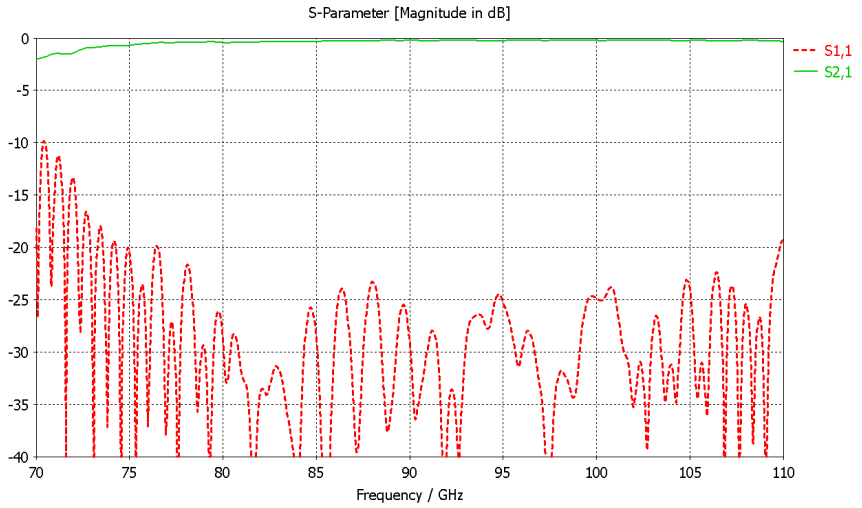

Figure 4.6: S-parameter plot for the horn and offset reflector wall in gap waveguide technology in a back-to-back configuration.

Fig. 4.7 and Fig. 4.8.

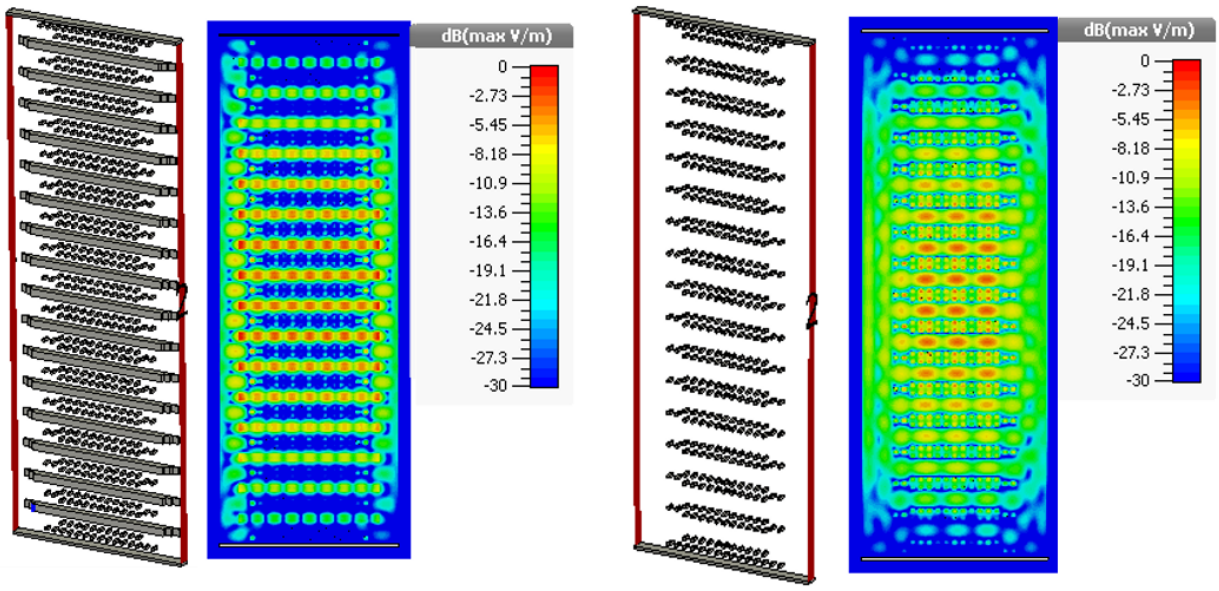

Figure 4.7: Various designs to couple waveport field inside the ridge (Left) and the groove (Right) based array of gap waveguides with their absolute average magnitude plot of the E-field component.

To solve this problem, fork shaped ridges have been implemented. In this concept, fork

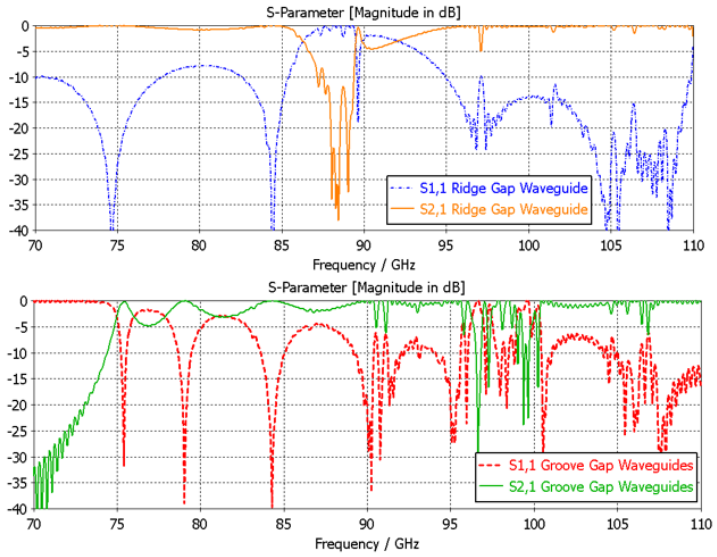

Figure 4.8: S-parameter with array of ridges (Top) and grooves (Bottom) in gap waveguide technology.

shaped transitions consist of steps that couple the fields from the aperture of the offset reflector wall or the equivalently large waveport into the ridge gap waveguide as shown in Fig. 4.9 where $L_1 = 0.7821$ mm, $L_2 = 0.68$ mm, $L_3 = 1.25$ mm, $h_1 = 0.15$ mm, $h_2 = 0.52$ mm, $h_3 = 0.89$ mm, $W_1 = 0.537$ mm , $W_2 = 0.774$ mm, and $S_1 = 0.774$ mm. The reason for the fork-shaped transition is that it hides the pins of the waveguide walls as much as possible and minimizes the exposure of the sides of pins of the waveguide to avoid very strong reflections. After many optimizations involving the positioning of the pins between forks, the EM fields manage to propagate into the ridged waveguide.

It can be seen from the Fig. 4.10 that the planar EM fields that are transmitted from the parabolic reflector wall couple with the fork shaped steps and propagate inside the waveguides. Similarly, it leaves the waveguides to enter second port in the back-to-back structure. Insertion loss is very low as well as the reflection coefficient as can be seen in Fig. 4.11. S_{11} is less than -15 dB in the range of 74 Ghz to 109 GHz and low insertion loss due to PEC materials.

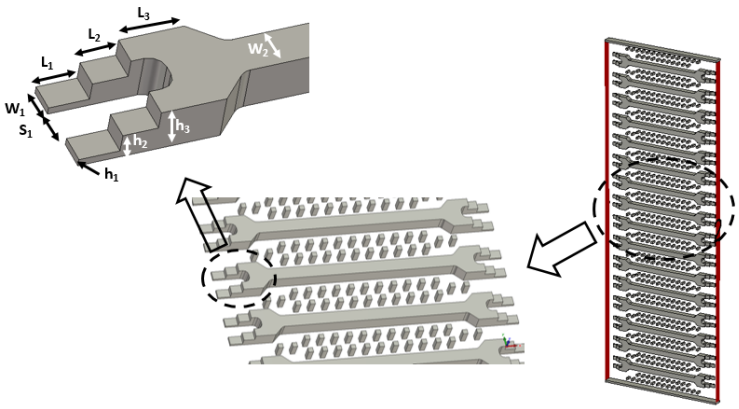

Figure 4.9: Fork-ridge-shaped transition based on the gap waveguide technology.

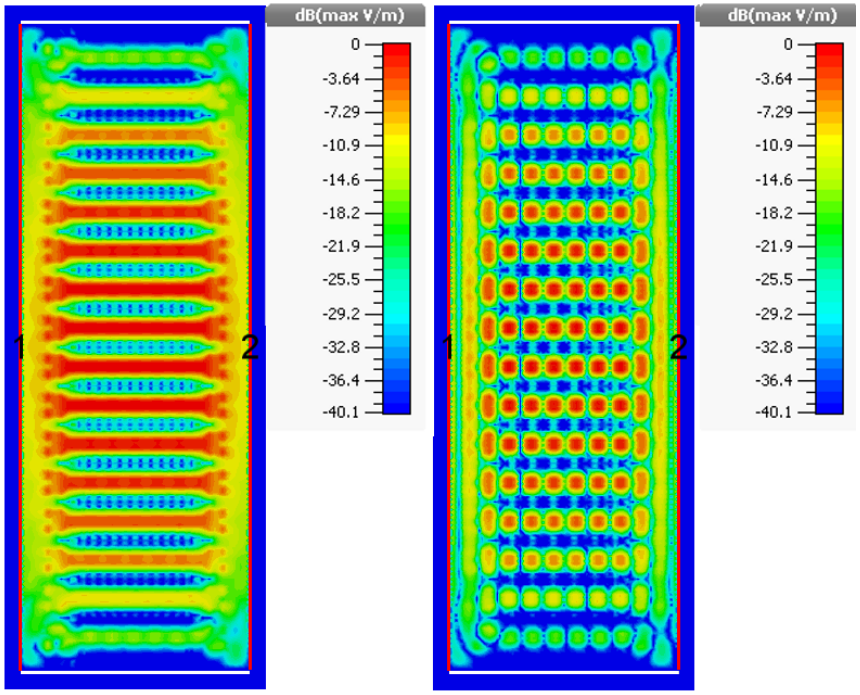

Figure 4.10: Absolute average magnitude plot (Left) and phase plot (Right) of E-field component with stepped-fork transitions.

4.3 Simulation of Back-to-Back structure consisting of Waveguides and Transitions

Ultimately, the transition and ridge-based array of waveguides are placed inside the back-to-back offset reflector wall structure (Section 4.1) as shown in Fig. 4.12. It has been

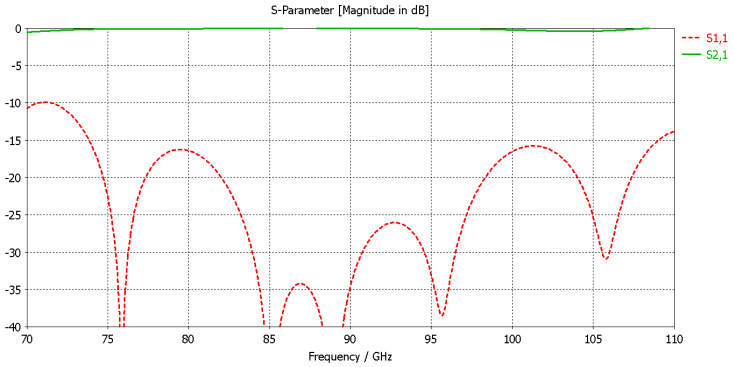

Figure 4.11: S-parameters for fork-ridge-shaped transition based on gap waveguide.

simulated by exciting one feed horn antenna (Left) while monitoring the received signal from the second horn antenna (Right) with electric boundary condition at the top and bottom side. E-Field pattern can be seen in Fig. 4.13. It shows that the amplitude pattern is tapered and that the field propagates with same phase at same time instant when approaching the forks. From Fig. 4.14, it can be seen that with the back-to-back structure is working very nicely in the whole band from 78 GHz to more than 110 GHz with on average of 0.5 decibels of insertion loss due to spillover where surface roughness is neglected.

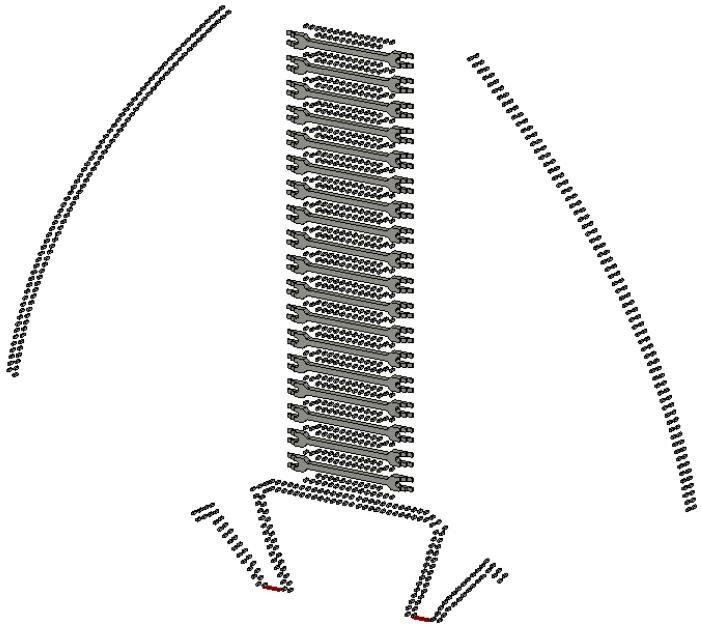

Figure 4.12: Back-to-back offset reflector wall structure with the fork transition.

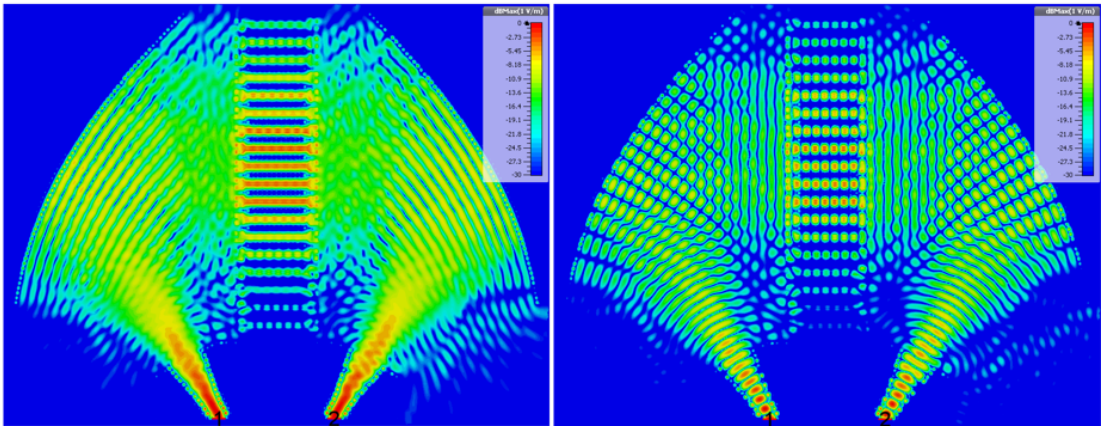

Figure 4.13: E-Field absolute magnitude (Left) and Phase (Right) plot in a back-to-back configuration at 80 GHz.

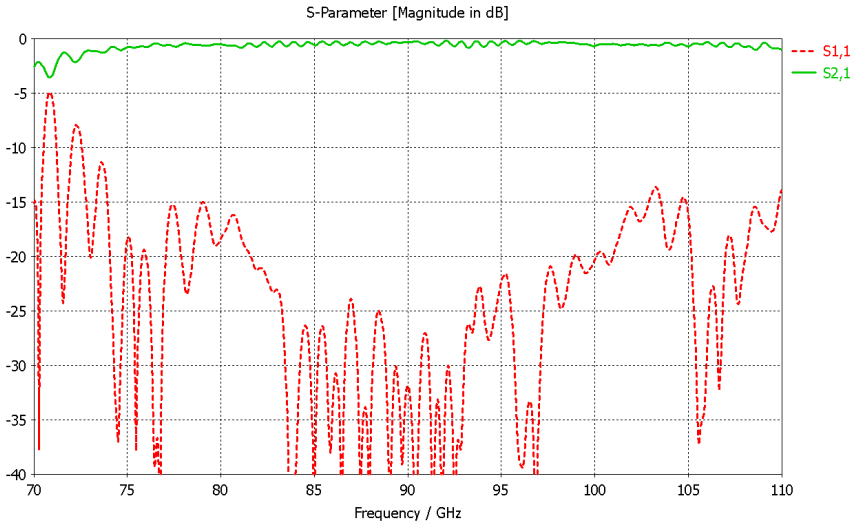

Figure 4.14: S-parameters plot of the complete back-to-back structure.

A power combiner/divider is generally characterized by its scattering parameter matrix that sets the relationships between the input and output waves at its external ports. To measure the total effect of power loss, i.e. due to reflections (and dissipation in non PEC materials), one can compute the radiation efficiency or maximum available power gain of this structure. For passive systems, the radiation efficiency (or passive gain) can take values from zero to one.

In this study, the maximum available power gain is referred to as passive gain G_{pass} and defined as the ratio of the output power P_{out} at the port of the receiving horn to the input

power P_{in} at the port of the transmitting horn feed where the input power is equal to the incident power P_{in}, which is reduced by the reflected power P_{ref}.

$$G_{\text{pass}} = \frac{P_{\text{out}}}{P_{\text{in}}} = \frac{P_{\text{out}}}{P_{\text{inc}} - P_{\text{ref}}} = \frac{P_{\text{inc}} \, |S_{21}|^2}{P_{\text{inc}} - P_{\text{inc}} \, |S_{11}|^2} = \frac{|S_{21}|^2}{1 - |S_{11}|^2} \tag{4.1}$$

It should be noted that this definition accounts for power losses due to the leakage in the gap waveguide structure (between the pins), spillover effects (when a fraction of feed's radiated power is not capture by the reflector), and Ohmic power losses (in the of non-PEC materials). However, internal reflection effects, for example due to non-uniform field illumination of the ridge waveguides, are not accounted for by this figure of merit. For this purpose, one can adopt illumination efficiency, which is commonly used in reflector antennas to measure the difference between the ideal uniform field distribution and the realized one by a practical feed. To evaluate the illumination efficiency (from now on referred to as uniformity efficiency) for the designed power combiner/divider, we have used the definition in [43]. The equation for uniformity efficiency e_{uni} has been re-written for the voltages V that has been measured at the middle of ridged array:

$$e_{\text{uni}} = \frac{\left| \sum_{n=1}^{N} V_n \right|^2}{N \sum_{n=1}^{N} |V_n|^2} \tag{4.2}$$

By using (4.1) and (4.2), the passive gain and uniformity efficiency have been computed and are plotted in Fig. 4.15.

The amplitude and phase imbalance of the fields has been measured at the center points of the ridge gap waveguides during the simulations using voltage monitors as shown in Fig. 4.16 and Fig. 4.17 respectively. As one can see, the amplitude and phase variations are within, respectively, 3 dB and 0.08^o over frequency band.

4.4 Conclusion

With the design of the fork shaped transition between the offset reflector wall and the array of ridge waveguides, we have achieved the desired level of coupling of the EM fields from the reflector to the waveguides. The relative field illumination taper at the edges of the reflector is very low (-21 dB) in magnitude. This spatial power combining and divider

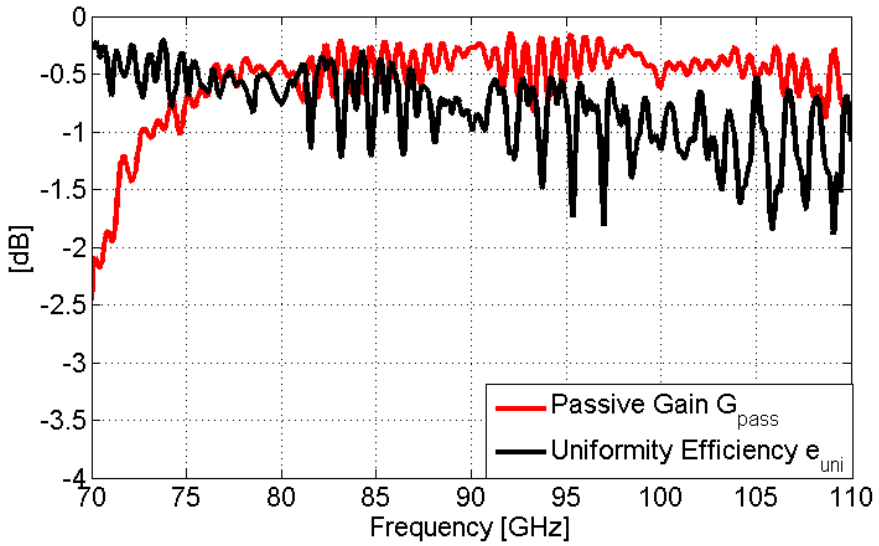

Figure 4.15: Passive gain plot for the back-to-back struture.

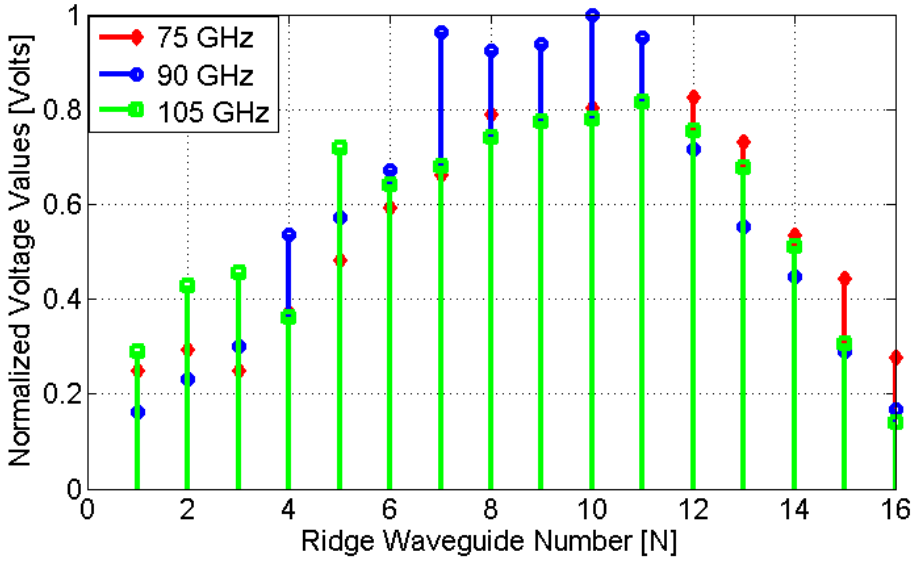

Figure 4.16: Amplitude imbalance/difference at the centers of the waveguides.

does not yet include a microstrip transition-line which renders it very wide bandwidth, essentially covering the entire W-band.

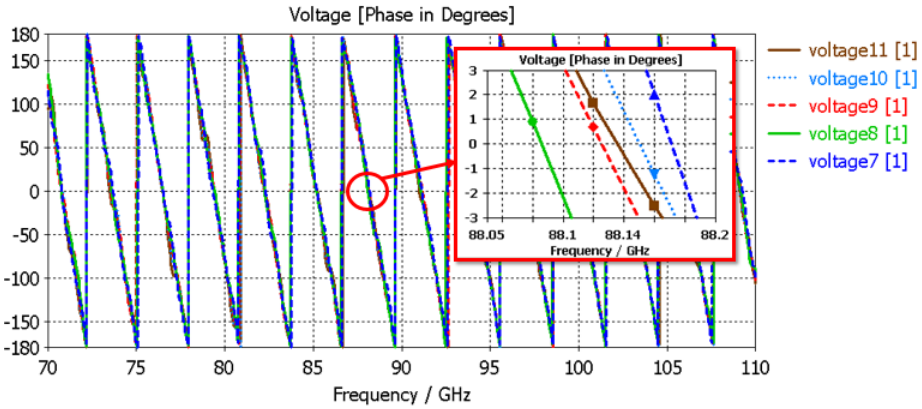

Figure 4.17: Phase imbalance plot at the center of the waveguides.

Chapter 5

Re-Design for Prototyping, Manufacturing, and Test Results

In this chapter, a prototype back-to-back structure has been designed that has been manufactured and tested. The Transmitting and receiving feeds oppose each-other due to the measurement setup at mm-wave frequencies. For the manufacturing, additional guiding pins and standard flange holes have been made. Testing has been done in complete W-band. The reflection coefficient and insertion loss has been measured during testing. Structure has been simulated again with changed conductivity value of the Aluminium due to surface roughness.

5.1 The Prototype Design

The prototype has been re-designed to comply with both manufacturing as well as measurement setup constraints. The second feed and the corresponding offset reflector wall is rotated in such a way that second feed faces the first feed, so that the EM waves propagate to the opposite side as shown in Fig. 5.1. The current structure employs fewer waveguides as compared to the previous model in Chapter 4. This is because the 3 waveguides have been removed which were at the edges and outside of the aperture of the offset reflector wall. This structure has been simulated with PEC materials. The amplitude and phase patterns are shown in Fig. 5.2. The spillover from the reflector walls is at a magnitude of

-21 decibels, which is very low. Fig. 5.3 shows the S-parameters of the structure. The S_{11} is less than -10 decibels from 74 GHz to beyond 110 GHz, whereas the insertion loss is on average 0.5 decibels from 77 GHz up to and beyond 110 GHz.

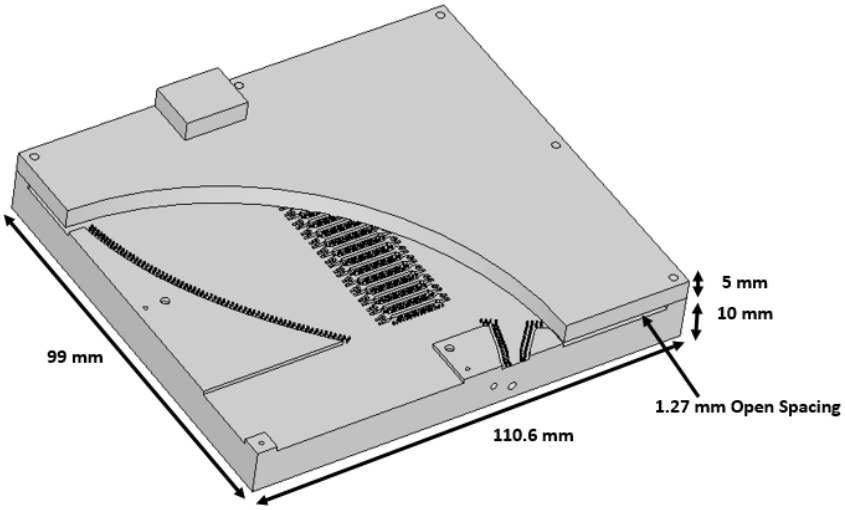

Figure 5.1: Back-to-back structure with PEC ground planes.

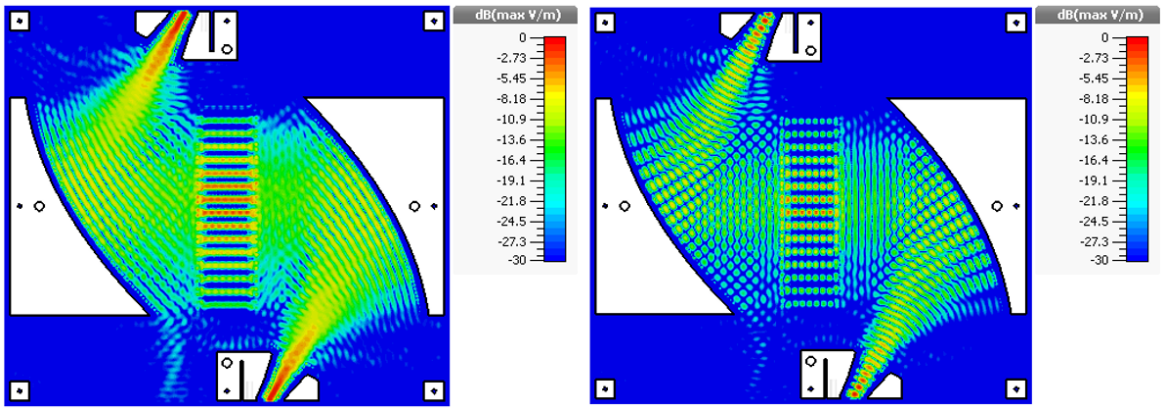

Figure 5.2: E-Field absolute average amplitude (Left) and Phase (Right) plot at 80 GHz in a back-to-back configuration with PEC ground planes.

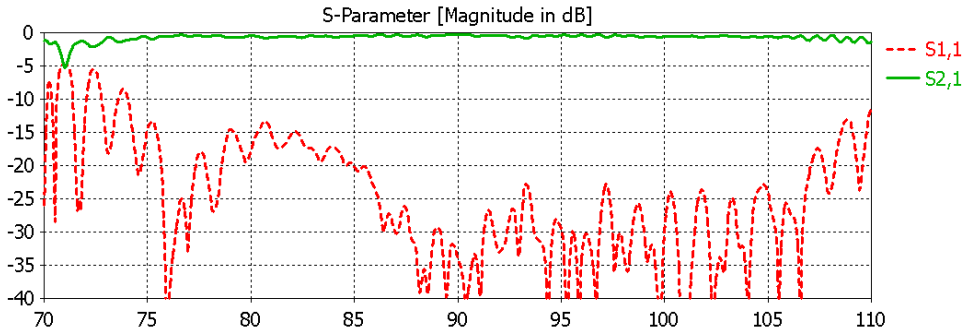

Figure 5.3: S-Parameter plot of back-to-back structure with PEC ground planes.

5.2 Manufacturing and Test Results

The prototype has been manufactured with the tolerances of 5-10 μm and using the Aluminium metal. In Fig. 5.4, the bottom ground plane of the prototype structure and the testing setup with the network analyzer has been shown. S-parameters has been measured within the operating band of 75-110 GHz as shown in the Fig. 5.5. It shows that the S_{11} is nearly same as with simulation results but S_{21} has degraded to -2.28 dB. The reason for degradation is the use of Aluminum metal and surface roughness around 10 μm in manufacturing. Prototype structure has been simulated again with the Aluminum metal

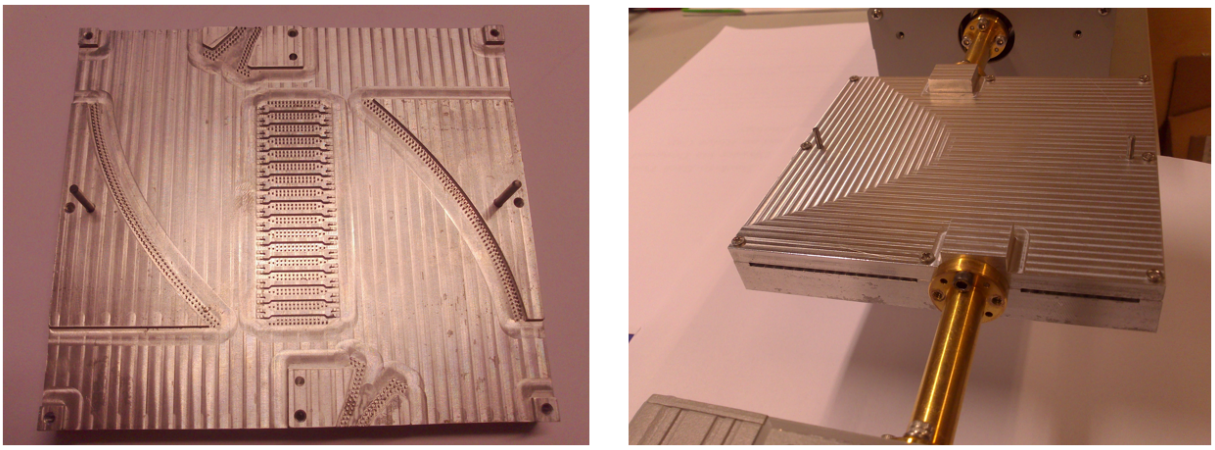

Figure 5.4: Manufactured prototype with bottom part (Left) and testing with the W-band waveguides connected to the network analyzer (Right).

material instead of PEC and 15 μm surface roughness has been added as well. It gave the same results like manufactured prototype which has been compared as shown in Fig.

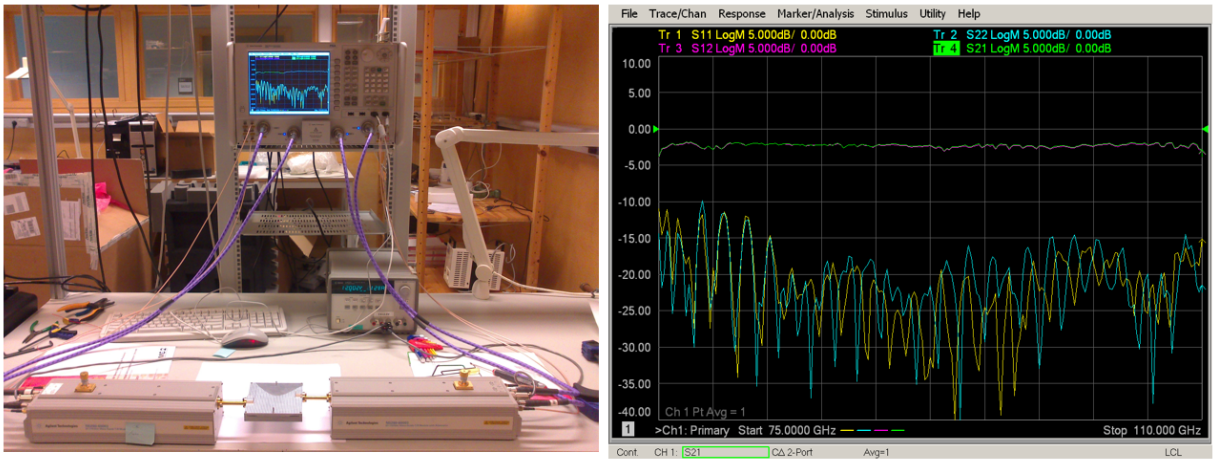

Figure 5.5: Complete testing setup with network analyzer (Left) and S-parameter results (Right).

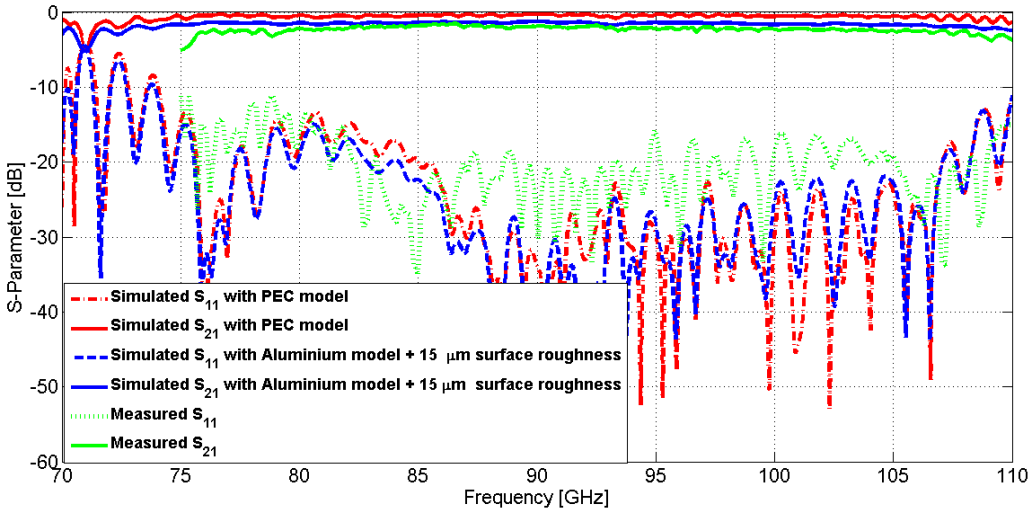

Figure 5.6: S-Parameter comparison of the prototype measurement with simulation results of PEC and Aluminium material structure.

5.6. Simulated results show that with PEC structure, 0.65 dB insertion loss is with PEC material. The material of the structure has been changed to the Aluminium and 15 μm of the surface roughness is added in CST. This further added 1.02 dB of insertion loss. On average it has total 1.67 dB insertion loss. The measurement of the prototype revealed that on average it has 2.28 dB insertion loss between simulations. The Fig. 5.6, shows that $S_{11} < -10$ dB covers the frequency range from 74 GHz to 110 GHz. The measured

passive gain for the measured S-Parameters has been calculated. It shows that around 1.5 to 2 dB degradation in passive gain as compared to simulated results in Fig. 5.7. It is due to varying surface roughness and leakages between imperfect pins in the manufactured prototype.

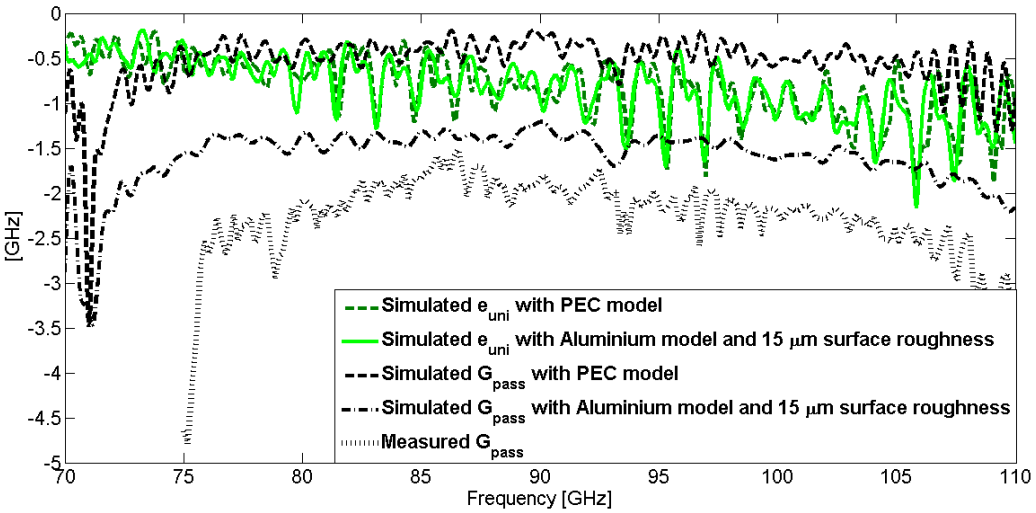

Figure 5.7: Measured total passive gain comparison with simulated plot.

5.3 Conclusion

In this chapter, structure has been re-designed, manufactured and tested in W-band range. The testing results shows that the there is only 0.65 dB insertion loss is with PEC material. The Aluminium metal and 15 μm surface roughness gives 1.67 dB insertion loss and 2.28 dB with measurements. S-parameters results shows that the prototype covers the whole W-band from 74-110 GHz for $S_{11} < -10$ dB.

Chapter 6

Conclusions and Recommendations

6.1 Conclusions

Initially, the EM waves has been analyzed by designing offset reflector wall in receiving mode. The EM fields which are converged on the focal point has been analyzed and helped in the designing of the feed for the offset reflector wall. The analysis showed that 83.85% power is received at 1λ radial distance position from the focal point.

Another analysis has been done in the receiving mode. In this analysis, the optimal excitation coefficients have been identified for the waveguides and the power captured at the focal point has been determined. The power received using optimal excitation coefficients has the same results when the waveguides were excited with equal magnitudes and phases.

The offset feed for the offset reflector wall has been designed. Then, propagation of EM fields between offset reflector wall and array of ridge waveguide was made possible with the help of fork shaped stepped transition. It played an important role to couple the fields inside the waveguides, covered the whole W-band.

Finally, the prototype has been manufactured and tested in W-band range. The measured S_{11} remains below -10 dB and insertion loss of 2.28 dB over the whole W-band from 74-110 GHz for the manufactured prototype. It has been identified with simulations and compared

to the measurements that insertion loss of 0.65 dB is with PEC structure and 1.67 dB when Aluminium metal and 15 μm surface roughness is added to the simulation. The simulated and measured prototype gave the same results as expected and covers the required band of interest.

6.2 Recommendations

This work is based on single feed spatial power combiner and divider designed ridge gap waveguide technology. This work can be the base for the future work with the following recommendations:

- The fields on the ridges can be amplified by using amplifiers. Method for coupling from ridge to MMIC amplifier needs to be studied.
- Any new method can be proposed to make equal amplitude levels at the ridges instead of tapered amplitude distribution of EM fields.
- Slot array antenna can be designed on the ridge part of the waveguides with amplifiers and more than one horn feed can be used for beam scanning for the slot array antenna.

Appendix A

In this appendix we prove that $\frac{1}{2}\mathrm{Re}\{\underline{W}^T P \underline{W}^*\} = \frac{1}{4}\underline{W}^H \mathrm{Re}\{P\}^T \underline{W}$. We can write that

$$\frac{1}{2}R_e\{\underline{W}^T P \underline{W}^*\} = \frac{1}{4}(\underline{W}^T P \underline{W}^* + (\underline{W}^T P \underline{W}^*)^H) = \frac{1}{4}(\underline{W}^T P \underline{W}^* + \underline{W}^T P^H \underline{W}^*)$$

$$= \frac{1}{4}(\underline{W}^T (P + P^H)\underline{W}^*) = \frac{1}{2}(\underline{W}^T \mathrm{Re}\{P\}\underline{W}^*) \tag{A.1}$$

Next we take the transpose of a scalar, which is the scalar itself, i.e.,

$$[\frac{1}{2}\mathrm{Re}\{\underline{W}^T P \underline{W}^*\}]^T = \frac{1}{2}(\underline{W}^T \mathrm{Re}\{P\}\underline{W}^*)^T$$

$$= \frac{1}{4}\underline{W}^H \mathrm{Re}\{P\}^T \underline{W}$$

which concludes the proof.

Bibliography

[1] J. W. Mink, "Quasi-optical power combining of solid-state millimeter-wave sources," *IEEE Trans. Microwave Theory Tech.,* vol. 34, no. 2, pp. 273-279, Feb. 1986.

[2] R.A. York and Z.B. Popovic, "Active and Quasi-Optical Arrays for Solid-State Power Combining." *New York: Wiley*, April 1997.

[3] M. P. DeLisio and R. A. York, "Quasi-optical and spatial power combining," *IEEE Trans. Microwave Theory Tech.,* vol. 50, no. 3, pp. 929-936, March 2002.

[4] R. A. York, "Some considerations for optimal efficiency and low noise in large power combiners", *IEEE Trans. Microwave Theory Tech.,* vol. 49, pp. 1477-1482, Aug. 2001.

[5] J. S. H. Schoenberg and Z. B. Popovic, "Planar lens amplifier", *IEEE MTT-S Int. Microwave Symp. Dig.,* pp. 429-432, May 1994.

[6] A. Alexanian and R. A. York, "Broad-band spatially combined amplifier array using tapered slot transitions in waveguide", *IEEE Microwave Guided Wave Lett.,* vol. 7, pp. 42-44, Feb. 1997.

[7] J. J. Sowers, D. J. Pritchard, A. E. White, W. Kong, O. S. A. Tang, D.R. Tanner, and K. Jablinskey, "A 36 W, V-band, solid-state source", *IEEE MTT-S Int. Microwave Symp. Dig.,* pp. 235-238. Jun. 1999.

[8] N. -S. Cheng, P. Jia, D. B. Rensch, and R. A. York, "A 120-W X-band spatially combined solid-state amplifier", *IEEE Trans. Microwave Theory Tech.,* vol. 47, pp. 2557-2561, Dec. 1999.

[9] S. Ortiz, J. Hubert, E. Schlecht, L. Mirth, and A. Mortazawi, "A 25 watt and a 50 watt Ka-band quasi-optical amplifier", in *IEEE MTT-S Int. Microwave Symp. Dig.,* vol. 2, pp. 797-800, Jun. 2000.

[10] B. Deckman, D. S. Deakin, E. Sovero, and D. Rutledge, "A 5-watt, 37-GHz monolithic grid amplifier", in *IEEE MTT-S Int. Microwave Symp. Dig.,* vol. 2, pp. 805-808, Jun. 2000.

[11] H. T. Than , G. W. Sun , G. S. Cuellar , J. Zeng , N. T. Schultz , M. E. Moya , Y. Chung , B. C. Deckman and M. P. DeLisio "A 600-W C-band amplifier using spatially combined GaAs FETs", *IEEE Compound Semiconductor IC Symp.,* vol. 1, Oct. 2011.

[12] Leggieri A, Paolo F., and Passi D. "Thermal and solid-mechanics FEM simulation of a microwave spatial power combiner amplifier", *COMSOL conf.,* vol. 3, pp. 1871-1874, June 2003.

[13] Y. J. Yu Cheng, W. Hong, and K. Wu "Millimeter-wave substrate integrated waveguide multibeam antenna based on the parabolic reflector principle", *IEEE Trans. Antennas Propag.,* vol. 56, vol. 9, pp. 3055-3058, Sep. 2008.

[14] Boccia, L., A. Emanuele, E. Arnieri, A. Shamsafar, and G. Amendola, "Substrate integrated power combiners", *Proc. 6th Eur. Conf. Antennas Propag.,* pp. 3631-3634, Mar. 2012.

[15] P.-S. Kildal, E. Alfonso, A.Valero-Nogueira, and E.Rajo-lglesias, "Local metamaterial-based waveguides in gaps between parallel metal plates", *IEEE Antennas and Wireless Propagation Letters.*, vol. 8, Apr. 2009.

[16] D. B. Rutledge, N. S. Cheng, R. A. York, R. M. Weikle, II, and M. P. De Lisio, "Failures in power-combining arrays", *IEEE Trans. on Microwave Theory and Techniques,* vol. 47, pp. 1077-1082, Jul. 1999.

[17] A. U. Zaman and P. -S. Kildal, "Wide-Band Slot Antenna Arrays With Single-Layer Corporate-Feed Network in Ridge Gap Waveguide Technology", *IEEE Trans. Antennas Propag.,* vol. 62, vol. 6, pp. 2992-3001, Jun. 2014.

[18] "FCC opens 70, 80, and 90 GHz Spectrum Bands for Deployment of Broadband Millimeter-wave Technologies", *FCC announcement,* WT Docket No. 02-146, Oct. 2003.

[19] A. Valero-Nogueira, E. Alfonso, J. I. Herranz, P.-S. Kildal, "Experimental demonstration of local quasi-TEM gap modes in single hard-wall waveguides", *IEEE Microwave and Wireless Comp. Lett.,* vol. 19, pp. 536-538, Sept. 2009.

[20] A. U. Zaman , P. -S. Kildal , M. Ferndahl and A. Kishk, "Validation of ridge gap waveguide performance using in-house TRL calibration kit", *Proc. 4th Eur. Conf. Antennas Propag.,* pp. 1-4, 2010.

[21] P.-S. Kildal, "Artificially soft and hard surfaces in electromagnetics", *IEEE Transaction on Antennas and Propagation,* vol. 38, pp. 1537-1544, Oct. 1990.

[22] P.-S. Kildal and A. Kishk, "EM modeling of Surfaces with STOP or GO characteristics - artificial magnetic conductors and soft and hard surfaces", *Applied Computational Electromagnetics Society Journal,* vol. 18, pp. 32-40, Mar. 2003.

[23] E. Rajo-Iglesias and P.-S. Kildal, "Numerical studies of bandwidth of parallel plate cut-off realized by bed of nails, corrugations and mushroom- type EBG for use in gap waveguides", *IET Microw. Antennas Propag.,* vol. 5, pp. 282-289, Mar. 2011.

[24] P. -S. Kildal, "Three metamaterial-based gap waveguides between parallel metal plates for mm/submm waves", *Proc. 3rd Eur. Conf. Antennas Propag.*, pp. 28-32, Mar. 2009.

[25] A. U. Zaman and P.-S. Kildal "Ku-band linear slot-array inridge gapwaveguide technology", *Proc. 7th Eur. Conf. Antennas Propag.,* pp. 3078-3081, Apr. 2013.

[26] Alfonso Als, A. U. Zaman, P. -S. Kildal, "Ka-band gap waveguide coupled-resonator filter for radio link diplexer application", *IEEE Trans. Compon. Packag. Manuf. Technol.,* pp. 870879, 2013.

[27] Morteza Rezaee, A. U. Zaman, P. -S Kildal, "V-Band Groove Gap Waveguide Diplexer", *9th Eur. Conf. Antennas Propag.*, pp. 1-4, Apr. 2015.

[28] Rahiminejad S, Raza H, A. U. Zaman, Haasl S, Enoksson P and P. S, Kildal, "2013 Micro machined Gap Waveguides for 100 GHz Applications", *7th Eur. Conf. Antennas Propag.,* pp. 19358, Apr. 2013.

[29] A. U. Zaman and P. -S. Kildal, "Slot antenna in ridge gap waveguide technology", *Proc. 6th Eur. Conf. Antennas Propag.,* pp. 3243-3244, Mar. 2012.

[30] E. A. Alos, A. U. Zaman, and P.-S. Kildal, "Ka-Band Gap Waveguide Coupled-Resonator Filter for Radio Link Diplexer Application", *IEEE Trans. Compon., Packag. Manuf. Technol.,* vol. 3, pp. 870-879, 2013.

[31] A. Razavi, P. -S. Kildal, X. Liangliang, E. Alfonso, and H. Chen, "2x2-slot Element for 60GHz Planar Array Antenna Realized on Two Doubled-sided PCBs Using SIW Cavity and EBG-type Soft Surface fed by Microstrip-Ridge Gap Waveguide", *IEEE Trans. Antennas and Propaga.,* vol. 62, pp. 4564-4573. Sep 2014.

[32] Antonio Berenguer, Mariano Baquero-Escudero, Daniel Sanchez-Escuderos, Bernardo Bernardo-Clemente, and V. E. Boria-Esbert, "Low insertion loss 61 GHz narrow-band filter implemented with Groove Gap Waveguides", *Proc. Eur. Microw. Conf.,* pp. 191-194, Oct. 2014.

[33] A. Kishk, A. U. Zaman, and P. -S. Kildal, "Numerical Prepackaging with PMC lid - Efficient and Simple Design Procedure for Microstrip Circuits including the Packaging", *ACES Appl. Comput. Soc. J.,* vol. 27, pp. 389-398, May 2012.

[34] A. U. Zaman, M. Alexanderson, T. Vukusic, and P. -S. Kildal, "Gap Waveguide PMC Packaging for Improved Isolation of Circuit Components in High-Frequency Microwave Modules", *IEEE Trans. Compon. Packag. Manuf. Technol.,* vol. 4, pp. 16-25, 2014.

[35] E. Rajo-Iglesias, P. -S. Kildal, A. U. Zaman, and A. Kishk, "Bed of Springs for Packaging of Microstrip Circuits in the Microwave Frequency Range", *IEEE Trans. Compon. Packag. Manufact. Technol.,* vol. 2, pp. 1623-1628, 2012.

[36] S. Rahiminejad, A. U. Zaman, E. Pucci, H. Raza, V. Vassilev, S. Haasl, P. Lundgren, P. -S. Kildal, and P. Enoksson, "Micromachined ridge gap waveguide and resonator for millimeter-wave applications, *Sens. Actuators A, Phys.*, vol. 186, pp. 264-269, Oct. 2012.

[37] S. W. Lee and Y. Rahmat-Samii, "Simple formulas for designing an offset multibeam parabolic reflector", *IEEE Trans. Antennas Propagat.,* vol. 29, pp. 472-478, 1981.

[38] M. V. Ivashina, C.G.M. van t Klooster, "Focal Fields in Reflector Antennas and Associated Array Feed Synthesis for High Efficiency Multi-Beam Performances", *25th ESA Antenna Workshop on Satellite Antenna Technology, Noordwijk, The Netherlands*, Sept. 2002.

[39] M. V. Ivashina, C. G. M. vant Klooster, "Focal Field Analyses for Front-Fed and Offset Reflector Antenna", *IEEE IS AP, Columbus, OH,* Jun. 2003.

[40] Y. T. Lo and S. W. Lee, "Optimization of directivity and signal-to-noise ratio of an arbitrary antenna array", *IEEE Trans. Antennas Propagat.,* vol. 54, no. 8, pp. 1033-1045, Aug. 1966.

[41] M. V. Ivashina, O. Iupikov, R. Maaskant, W. van Cappellen, and T. Oosterloo, "An optimal beamforming strategy for wide-field surveys with phased-array-fed reflector antennas", *IEEE Trans. Antennas Propagat.,* vol. 59, no. 6, pp. 1864-1875, Jun. 2011.

[42] O. A. Iupikov, R. Maaskant, M. V. Ivashina, A. Young, and P. S. Kildal, "Fast and Accurate Analysis of Reflector Antennas with Phased Array Feeds including Multiple Reflections between Feed and Reflector", *IEEE Trans. Antennas Propagat.,* pp. 3450-3462, Apr. 2014.

[43] P. -S. Kildal, *Foundations of Antenna Engineering*, 2015: Compendium in Antenna Engineering at Chalmers.